

REMOTE ELECTRO-OPTICAL DETECTION OF
SINGLET OXYGEN IN VIVO

A REMOTE ELECTRO-OPTICAL TECHNIQUE FOR
MONITORING SINGLET OXYGEN GENERATION
DURING PHOTODYNAMIC THERAPY

By

STEEN J. MADSEN, B.Sc.

A Project

Submitted to the School of Graduate Studies
in Partial Fulfilment of the Requirements
for the Degree
Master of Science
(Health and Radiation Physics)

McMaster University

July 1988

MASTER OF SCIENCE (1988)
(Health and Radiation Physics)

McMASTER UNIVERSITY
Hamilton, Ontario

TITLE: A Remote Electro-optical Technique for
Monitoring Singlet Oxygen Generation During
Photodynamic Therapy

AUTHOR: Steen J. Madsen, B.Sc. (University of Toronto)

SUPERVISOR: Dr. M.S. Patterson

NUMBER OF PAGES: x, 107

ABSTRACT

Photodynamic therapy (PDT) is a form of local cancer treatment in which cell death is caused by photochemical reactions involving an exogenous photosensitizer. The photosensitizer, which is preferentially retained in malignant tissues, is photoactivated and cell death results from the generation of reactive products - most likely excited molecular (singlet) oxygen. The development of in vivo PDT dosimetry would be greatly aided by the ability to directly measure the local concentration of this product by non-invasive means.

In condensed media singlet oxygen will, with some small probability, undergo a radiative transition to the ground state with emission at 1270 nm. This infrared phosphorescence may provide a means for monitoring the production of singlet oxygen in vivo. Unfortunately the background infrared fluorescence observed from tissue may be many times the expected magnitude of the 1270 nm phosphorescence, even within the bandwidth encompassing the peak.

The principal aim of this project was the design of

a system optimized for the in vivo detection of the singlet oxygen emission. The system makes use of the most sensitive commercially available detector and uses phase sensitive detection to discriminate against infrared fluorescence. The system's performance matched theoretical expectations for the photosensitizer Photofrin II in aqueous and methanol solutions. However, a discrepancy in the observed and theoretical values was noted for aluminum chlorosulphonated phthalocyanine suggesting a deviation from simple first order kinetics. Singlet oxygen phosphorescence was not observed during PDT of cell suspensions or mouse tumours even though considerable cell death and tumour necrosis were observed.

The most likely explanation of this failure is that, due to quenching by biomolecules, the lifetime of singlet oxygen in cells or tissue is much lower than in solution so that the probability of emission is reduced accordingly. Quantitative calibration of the system yielded a lower limit of approximately $0.1 \mu\text{s}$ on the singlet oxygen lifetime in tissue. This suggests that singlet oxygen is generated in a protein environment.

ACKNOWLEDGEMENTS

It is with great pleasure that I acknowledge the contribution of Dr. Patterson to this project. The patience with which he answered my questions and his willingness to spend long hours in the lab were greatly appreciated.

I would also like to thank Stephen Flock for his help and advice during the course of this project. His companionship during the sweltering summer evenings spent in our office made writing this project bearable.

I would also like to express my gratitude to; Dr. Wilson for many thought provoking discussions; Paula Deschamps and Karen Peterson for their help in carrying out the biological experiments; John Blenkey and Scott Phillips for making equipment which was invaluable to this work; James Stang for his computing help; Frank Sheridan for repairing faulty electronic components and Joel Zeger and Diane Burns for explaining the intricacies of dye laser tuning.

Thanks also goes to my parents for their support and encouragement throughout the course of this project.

TABLE OF CONTENTS

	<u>Page</u>	
CHAPTER 1	INTRODUCTION	1
	1.1 Cancer	1
	1.2 A brief overview of the photodynamic therapy process	2
	1.3 Singlet oxygen	4
	1.4 Project proposal	7
	1.5 Detection of singlet oxygen	10
CHAPTER 2	THEORY	13
	2.1 Production of the 1270 nm 1O_2 emission	13
	2.1.1 Triplet photosensitized production of 1O_2	13
	2.1.2 Deactivation of 1O_2	16
	2.2 An electro-optical system for 1O_2 detection	19
CHAPTER 3	MATERIALS AND METHODS	27
	3.1 Instrumentation	27
	3.1.1 Description of system	27
	3.1.2 Optimization of optical output and detector input	36
	3.1.3 Lock-in detection procedure	41
	3.2 Sample preparation and	

Table of Contents (cont.)

	<u>Page</u>
experimental set-up	43
3.2.1 Solution experiments	43
3.2.2 Cell suspension experiments	47
3.2.3 In vivo experiments	48
CHAPTER 4 RESULTS AND DISCUSSION	51
4.1 Evaluation of the system performance	51
4.2 Detection of 1O_2 in solution	54
4.2.1 Introduction	54
4.2.2 Detection of 1O_2 in MeOH and PBS using PFII	57
4.2.3 Detection of 1O_2 in MeOH and PBS using AlSPc	65
4.3 Detection of 1O_2 in vivo	72
4.3.1 Introduction	72
4.3.2 1O_2 detection in mice injected with PFII	72
4.4 Detection of 1O_2 in protein-aqueous solution	77
4.4.1 Introduction	77
4.4.2 Detection of 1O_2 in a 10 % solution of FCS and PBS using PFII ($50 \mu\text{g ml}^{-1}$)	77
4.4.3 Detection of 1O_2 in a 10 % solution of FCS and PBS using AlSPc ($2 \mu\text{g ml}^{-1}$)	80

Table of Contents (cont.)

	<u>Page</u>
4.5 Detection of $^{10}\text{O}_2$ in cell suspensions	82
4.5.1 Introduction	82
4.5.2 Detection of $^{10}\text{O}_2$ in cell suspensions using PFII and AlSPc	83
4.6 Estimation of the $^{10}\text{O}_2$ lifetime in vivo	91
4.7 Future developments	94
CHAPTER 5 CONCLUSIONS	96
APPENDIX A DERIVATION OF DETECTOR RESPONSE	99
REFERENCES	103

LIST OF FIGURES

<u>Figure</u>		<u>Page</u>
1.1	Molecular orbitals for oxygen formed from 1s, 2s, and 2p atomic orbitals.	5
1.2	Potential energy curves for the three lowest electronic states of molecular oxygen.	8
2.1	Production of singlet oxygen involving reactions between excited photosensitizer and triplet ground state oxygen.	14
3.1	System schematic.	28
3.2	Illustrations of diffraction efficiency and extinction ratio.	30
3.3	Overhead view of ADM assembly plate.	33
3.4	Sketch of filter pass bands and 1O_2 emission spectrum.	37
3.5	In vitro geometry.	44
3.6a	Absorption spectrum of AlSPc in MeOH ($50 \mu\text{g ml}^{-1}$).	46
3.6b	Absorption spectrum of PFII in MeOH ($50 \mu\text{g ml}^{-1}$).	46
3.7	In vivo geometry.	50
4.1	Detector sensitivity and noise versus chopping frequency.	52
4.2	Spectral response of the E0-817S.	55
4.3	NEP versus chopping frequency.	56
4.4	Normalized in-phase and quadrature outputs versus chopping frequency (PFII in MeOH).	59

List of Figures (cont.)

<u>Figure</u>		<u>Page</u>
4.5	Normalized quadrature outputs versus chopping frequency for AlSPc in PBS and in MeOH.	66
4.6	Normalized in-phase outputs versus chopping frequency for AlSPc in PBS and in MeOH ($2 \mu\text{g ml}^{-1}$).	67
4.7a	1272 nm quadrature outputs in vivo versus chopping frequency.	73
4.7b	1303 nm quadrature outputs in vivo versus chopping frequency.	73
4.8	Soret band absorption spectra of PFII in various solutions ($5 \mu\text{g ml}^{-1}$).	79
4.9	Normalized quadrature outputs versus chopping frequency for AlSPc in various solutions.	81
A1	Impulse response of the E0-817S.	101
A2	Semilog plot of E0-817S response.	102

CHAPTER 1

INTRODUCTION

1.1 Cancer

Cancer is the second leading cause of death in Canada accounting for approximately 51 000 deaths in 1987. The high mortality rate can be attributed to the fact that cancers grow rapidly and readily disseminate throughout the body. The causes of cancer are probably many and varied, however, the most likely include viruses, environmental factors and aberrant genes (Tannock and Hill 1987).

At present there are three standard treatment modalities which are used either singly or in combination: surgery, radiotherapy and chemotherapy. The efficacy of these treatments depends on numerous factors and the prognosis for cure varies from poor to excellent. Obviously then, there is a need for better cancer therapy.

In spite of the ability of cancers to disseminate throughout the body, it has been found that local tumour control leads to an improved prognosis (Suit 1982), and certainly can alleviate symptoms resulting in a better quality of life. Photodynamic therapy is an experimental form of cancer therapy which has recently shown promise in

providing local control of some cancers (Wilson and Jeeves 1987).

1.2 A brief overview of the photodynamic therapy process

The term "photodynamic" refers to biological change caused by the photochemical products of light-activated photosensitizers in the presence of oxygen. As applied in oncology, photodynamic therapy (PDT) is a tool for management of cancer patients with localized, small tumours.

PDT is essentially a two-step process. A photosensitizer is first administered intravenously, then, after a delay of 1 to 3 days to allow accumulation in the tumour tissue, the target volume is irradiated with visible light at a wavelength matching one of the absorption peaks of the photosensitizer. For example, when using haematoporphyrin derivative (HPD), the excitation wavelength is in the red portion of the spectrum (approximately 630 nm). HPD was the first photosensitizer to be widely used clinically but a purified version, known as Photofrin II (PFII), is now most commonly employed. PFII is a mixture of several different porphyrins, however, its attractiveness lies in the fact that it is rich in dihaematoporphyrin ether (DHE) which contains all the

tumour localizing and photosensitizing activity (Dougherty 1984). In spite of its widespread use in PDT, PFII is far from ideal. Since it is a mixture of several different porphyrins, reproducibility is a problem. Furthermore, tumour selectivity is relatively poor and the side effects, primarily cutaneous photosensitivity, can be unpleasant. Perhaps the greatest drawback with PFII is its weak absorption peak in the red portion of the spectrum where tissue penetration is high. In response to these problems, a new group of non-porphyrin photosensitizers (the phthalocyanines) has recently come under close scrutiny (Spikes 1986). These photosensitizers may be useful in PDT due to their strong absorption in the red portion of the spectrum. Aluminum chlorosulphonated phthalocyanine (AlSPc) is one of many of these new photosensitizers which is currently being investigated for use in PDT.

As a result of light absorption, the photosensitizer is raised to an excited state. One mode of sensitizer de-excitation involves energy transfer to ground state triplet molecular oxygen, producing molecular oxygen in an excited singlet state. It is this "singlet oxygen" that is thought to be responsible for the majority of cell death in PDT (Weishaupt et al. 1976). Cell death is most likely caused by the interaction of singlet oxygen with essential biomolecules such as certain amino acids and

nucleic acid bases, phospholipids, unsaturated lipids and proteins (Spikes and Bommer 1986).

1.3 Singlet oxygen

Oxygen is a very stable molecule since it is the only molecular element with a ground state that has triplet multiplicity (Rodgers 1985). Almost all substances that are to react with ground state molecular oxygen have singlet multiplicity. Spin selection rules forbid reactions between singlet and triplet states thus, in order for a reaction to occur, a change in multiplicity must take place. One way of accomplishing this is by inverting the spin of one of the oxygen electrons to generate one of the singlet states of oxygen (Rodgers 1985).

Using the Linear Combination of Atomic Orbitals (LCAO) approach, the combination of two oxygen atoms into an oxygen molecule results in the setting up of 10 distinct molecular orbitals (5 bonding and 5 antibonding) into which 16 electrons can be assigned with a maximum of 2 electrons per orbital (Figure 1.1). The lower energy orbitals in Figure 1.1 are filled first and when 14 electrons have been inserted, 3σ , 2π and $2\sigma^*$ orbitals are filled. The antibonding orbitals are denoted by stars in Figure 1.1. The two remaining electrons, each with a choice of an "up"

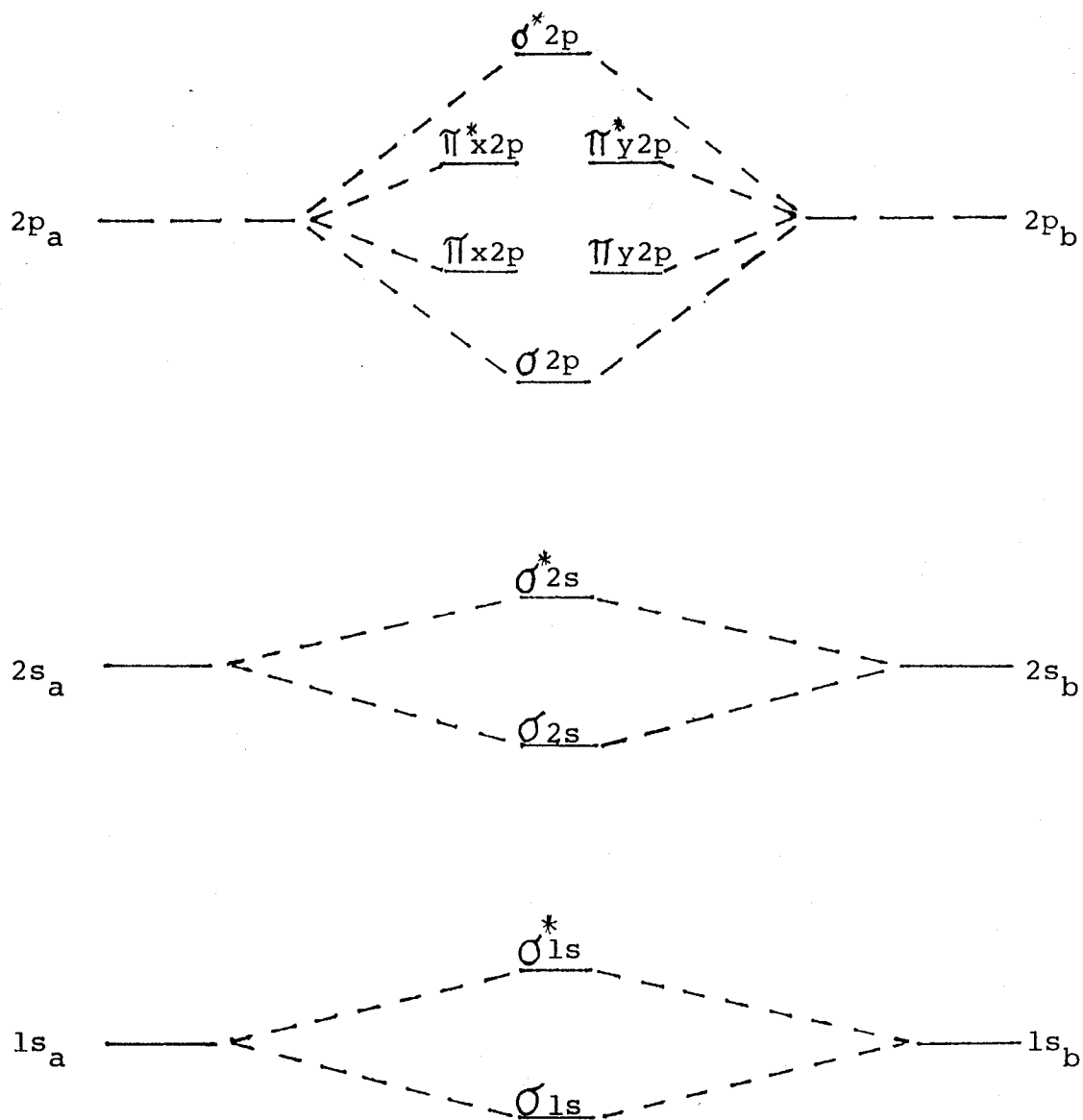
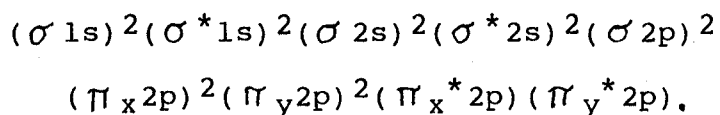


Figure 1.1 Molecular orbitals for oxygen formed from 1s, 2s, and 2p atomic orbitals (Levine 1983).

or "down" spin vector are placed into the degenerate π^* orbital pair resulting in six possible spin-orbital assignments:

$$\begin{aligned} & (\pi_{x^*} \downarrow \uparrow)^2, (\pi_{y^*} \uparrow \downarrow)^2 \\ & (\pi_{x^*} \uparrow) (\pi_{y^*} \downarrow), (\pi_{x^*} \downarrow) (\pi_{y^*} \uparrow) \\ & (\pi_{x^*} \downarrow) (\pi_{y^*} \uparrow), (\pi_{x^*} \uparrow) (\pi_{y^*} \downarrow) \end{aligned}$$

From these six spin-orbital assignments six independent electronic state components can be derived. The first pair shown correspond to the two components of the ${}^1\Delta$ state, with orbital angular momentum eigenvalue 2, and spin angular momentum eigenvalue 0. This state is generally referred to as "singlet oxygen" by organic chemists (Turro 1978). The next pair of assignments correspond to the +1 and -1 spin angular momentum components of the ${}^3\Sigma$ state, both with orbital angular momentum eigenvalue 0. The third pair of assignments correspond to 0 eigenvalue under both orbital and spin angular momentum operators. They can be represented by the ${}^1\Sigma$ term symbol (Frimer 1985). Since the term with the highest multiplicity is lowest in energy (Hund's rule), the ${}^3\Sigma$ state is the ground state. This agrees with the observed paramagnetism of ground state O_2 (Levine 1983). The electronic configuration of ground state O_2 can thus be written:



In subsequent discussions, the triplet ($^3\Sigma$) and singlet ($^1\Delta$) states of molecular oxygen will be referred to as 3O_2 and 1O_2 respectively.

The experimentally determined potential energy curves of the three electronic states are illustrated in Figure 1.2 (Turro 1978). From Figure 1.2 it can be seen that de-excitation of 1O_2 to 3O_2 may be accompanied by the emission of near-infrared photons at 1270 nm. As will be discussed below, this emission may provide a means of non-invasive in vivo PDT dosimetry.

1.4 Project proposal

The development of in vivo PDT dosimetry is still in its infancy. One of the major aims of present day PDT research is thus to develop reliable techniques which can be used in the quantitation of biological effects at the tumour level. Since 1O_2 is believed to be the primary cytotoxic species in PDT, it follows that the biological response to this form of therapy will depend on the local 1O_2 concentration at the tumour. This in turn depends on the light fluence rate, and on the photosensitizer and ambient oxygen concentration in the tumour. Therefore, an accurate calculation of the local 1O_2 concentration would require knowledge of these three parameters. Measurements

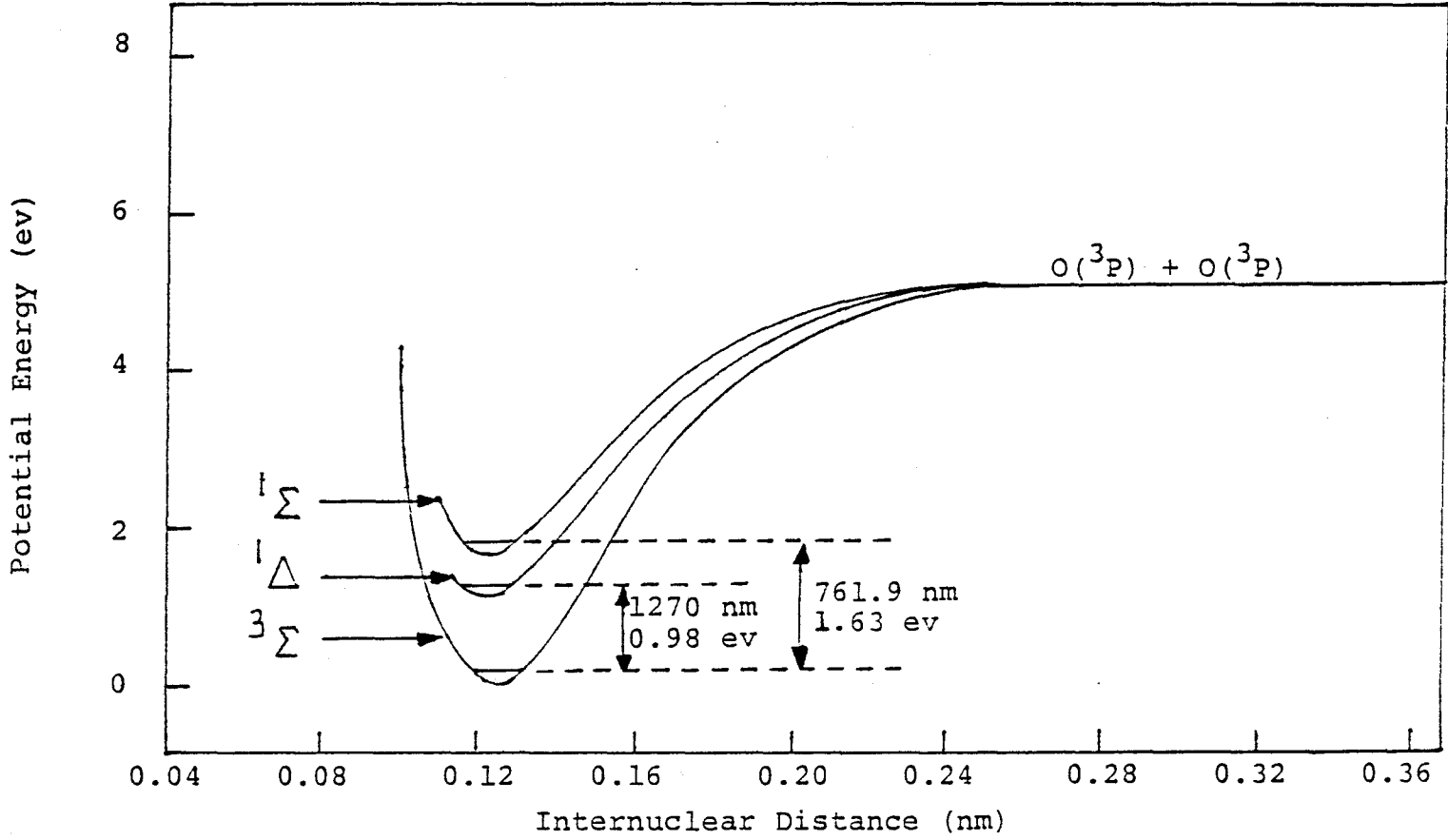


Figure 1.2 Potential energy curves for the three lowest electronic states of molecular oxygen (Turro 1978).

of these parameters are, however, non trivial. A more direct approach involves determination of the in vivo $^1\text{O}_2$ concentration via detection of near-infrared photons resulting from $^1\text{O}_2$ de-excitation. Such an approach is taken in this work.

The purpose of this project can be summarized in six steps:

- (1) develop a non-invasive, near-infrared detection system for monitoring the production of $^1\text{O}_2$.
- (2) determine the capability of the system for $^1\text{O}_2$ detection, i.e., determine the system sensitivity and noise.
- (3) monitor the production of $^1\text{O}_2$ in various organic and aqueous solutions and compare with theory.
- (4) monitor the production of $^1\text{O}_2$ in vivo using animal tumours and in vitro using cell suspensions.
- (5) compare the in vivo and in vitro results to those obtained using the solutions in order to learn something about the biological environment in which $^1\text{O}_2$ is produced.
- (6) obtain a lower limit of the $^1\text{O}_2$ lifetime in biological media.

1.5 Detection of singlet oxygen

Previous studies concerning the detection of $^1\text{O}_2$ in the liquid phase have relied almost exclusively on indirect methods. The most popular of these methods involves the use of chemical acceptors, or traps, which react selectively with $^1\text{O}_2$ but which are essentially inert to $^3\text{O}_2$. The use of such indicators is a problem for a number of reasons (Parker and Stanbro 1984):

- (i) concentration problems - too high a concentration leads to significant quenching and too little to serious indicator depletion.
- (ii) certain indicators react with both $^1\text{O}_2$ and free radicals in the same manner.
- (iii) acceptors tend to be either water soluble or lipid soluble, but not both.
- (iv) they cannot be used in vivo due to problems associated with their delivery to and removal from the tumour volume.

The detection of $^1\text{O}_2$ in solution by emission spectroscopy was not accomplished until the mid 1970s. This can be attributed to the unfavourable spectral location of its phosphorescence in the near-infrared where photomultipliers are ineffective and PbS or Ge semiconductor devices have relatively poor detectivity.

With the improvement of Ge diode detectors, $^1\text{O}_2$ emission measurements have become feasible and the contradictory data obtained earlier through the use of indirect methods have largely been resolved (Schmidt et al. 1987).

The first direct spectroscopic observation of the $^1\text{O}_2$ infrared ($^1\Delta, \nu=0 \rightarrow ^3\Sigma, \nu=0$) emission in dye sensitized solution was made by Krasnovsky (1976). This first direct attempt was rather crude due in large part to the poor detection systems available. Due to the fact that the photomultiplier used had very poor sensitivity in the near-infrared, Krasnovsky's observations must have been very close to the limits of detectability. Significant improvements in the direct measuring technique were made a few years later by Khan and Kasha (1979). They used a more sensitive near-infrared spectrophotometer that featured a thermoelectrically cooled PbS detector. These investigators were also the first to use HPD in direct spectroscopic investigations. The present day kinetic techniques involving pulsed laser excitation in combination with Ge semiconductor photodiodes were largely developed in the early 1980s (Parker and Stanbro 1984). However, optical monitoring of $^1\text{O}_2$ using a continuous wave, tunable dye laser as the excitation source and a lock-in detection technique was only recently developed by Parker (1987). This method of $^1\text{O}_2$ detection was used in this work.

Parker's continuous wave method was considered more feasible than a pulsed technique since the fast (short time constant) detectors needed for such an approach have poor sensitivity. Furthermore, the continuous wave method can easily be used to monitor $^1\text{O}_2$ emissions during treatment since the beam is only off for half the time and the treatment laser itself can be used for excitation.

CHAPTER 2

THEORY

2.1 Production of the 1270 nm 1O_2 emission

2.1.1 Triplet photosensitized production of 1O_2

The optical transitions and energy transfer processes involved in the photosensitized production of 1O_2 (using PFII) are summarized in Figure 2.1. The solid and dashed arrows represent radiative and radiationless transitions respectively. Absorption of 624 nm light causes the photosensitizer to make a transition from its ground singlet electronic state (S_0) to a higher electronic energy state with no spin change. The lifetime of this excited state (S_1) is very short, between 1 and 10 ns (Parker and Stanbro 1981). S_1 returns to S_0 by way of three deactivation paths (two direct and one indirect). The direct paths involve: (i) a radiationless transition, otherwise known as an internal conversion, in which the excess energy is lost to the surroundings as heat (very low probability), and (ii) a radiative transition involving emissions starting at 624 nm and continuing into the near-infrared - the so-called characteristic red porphyrin fluorescence occurring with low probability. The indirect path, occurring with high probability, involves an

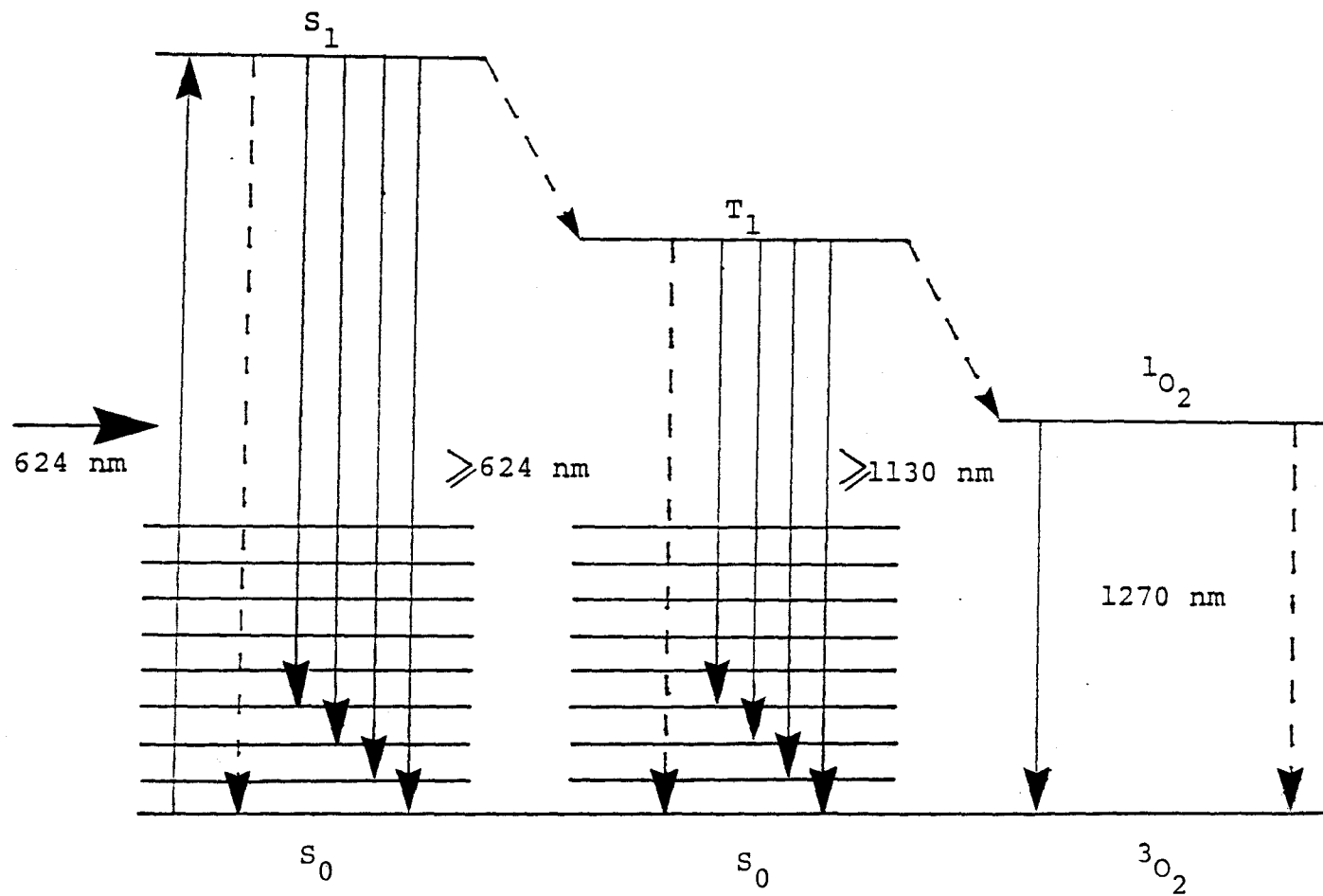
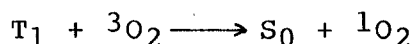


Figure 2.1 Production of singlet oxygen involving reactions between excited photosensitizer and triplet ground state oxygen.

intersystem crossing in which a transition from S_1 to the lowest allowed triplet state (T_1) takes place. The efficiency of T_1 formation depends on the particular sensitizer and solvent, but typically ranges from 0.3 to 0.8.

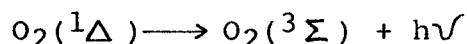
Deactivation from T_1 to S_0 occurs via three pathways. The first involves a non-radiative mechanism while the second involves a radiative transition. Since the energy of the T_1 state is approximately 1.1 eV (Boulnois 1986), the T_1 ($v = 0$) \rightarrow S_0 ($v = 0$) radiative transition yields photons in the near-infrared (1130 nm). However, transitions to higher vibrational energy levels of S_0 result in photons of wavelength comparable to those produced in 1O_2 deactivation. Fortunately, the infrared emissions are extremely small since the radiative (and non-radiative) transitions are forbidden by spin selection rules. The third (and most probable) deactivation pathway (in the presence of 3O_2) involves an energy transfer process. Since 3O_2 exists as a triplet in its ground state and as a singlet in its first excited state, it exists as a natural complement to the metastable dye. Thus, in the presence of 3O_2 , an intermolecular spin-conserving and energetically favourable interaction occurs where the dye molecule returns to its ground state while oxygen is raised to its first excited singlet state:



This energy transfer process is not the only method of triplet quenching by 3O_2 . Triplet porphyrins can also interact with 3O_2 to produce radicals such as the superoxide radical ($\overline{O}_2\cdot$) via an electron transfer process (Jori and Spikes 1984). The $\overline{O}_2\cdot$ yields are however quite low and its role in photodynamic cell destruction is not clear. In a few cases, triplet porphyrins will interact directly with biomolecules thus initiating other free radical processes. As a result, due to the production of $\overline{O}_2\cdot$ and other radicals through T_1 quenching and due to radiative and non-radiative T_1 to S_0 deactivation, the 1O_2 yield will be somewhat lower than the T_1 yield.

2.1.2 Deactivation of 1O_2

Of the numerous deactivation paths available to 1O_2 , only two are of importance to this work: (i) a highly forbidden, spontaneous radiative transition and (ii) a non-radiative, solvent-induced deactivation. Since 1O_2 is an unstable molecule it can, in the absence of collisions, spontaneously emit a photon:



This transition is however highly forbidden by spin and symmetry factors and in low pressure gases the lifetime is approximately 3600 s (Scurlock and Ogilby 1987). As illustrated in Figure 1.2, the emitted phosphorescence,

corresponding to the 0-0 vibrational transition, is in the near-infrared at 1270 nm. As previously mentioned, it is this spontaneous deactivation path which allows for remote optical monitoring in condensed phases. In contrast to the gas phase (at very low pressure) where the radiative route dominates, the non-radiative route is almost entirely responsible for $^1\text{O}_2$ relaxation in solution. For example, the ratio of the $^1\text{O}_2$ lifetime in water (3.2 μs - Parker 1987) to the radiative lifetime in water (4.0 s - Parker 1987) is approximately 10^{-6} . Thus only 1 in 10^6 $^1\text{O}_2$ molecules will deactivate via the radiative pathway. In condensed phases then, the $^1\text{O}_2$ signal will be extremely weak. By providing an alternative pathway for $^1\text{O}_2$ deactivation, solvation drastically reduces the $^1\text{O}_2$ lifetime. Since non-radiative processes depend on the nature of the solvent, the $^1\text{O}_2$ lifetime will depend on the particular solvent involved. For example, the lifetime of $^1\text{O}_2$ in MeOH (10.4 μs) is approximately three times greater than in water (Rodgers 1985). This large solvent effect can be explained in terms of electronic - to - vibrational energy transfer. Briefly, $^1\text{O}_2$ reaches its ground state by transferring electronic energy to vibrational oscillators in the adjacent solvent molecules. The coupling efficiency of this process, and hence the $^1\text{O}_2$ lifetime, depends on the highest frequency vibrational

mode of the solvent molecules. In this case then, the solvent acts as an energy acceptor in its interaction with $^1\text{O}_2$ (Hurst and Schuster 1983).

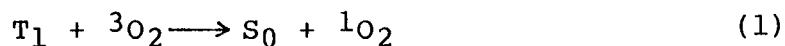
The weakness of the $^1\text{O}_2$ phosphorescence poses a problem since the sensitizer emits at the same wavelength (Figure 1.2). In vitro, this sensitizer infrared fluorescence may exceed the $^1\text{O}_2$ phosphorescence by as much as ten fold (Parker 1987). The problem is compounded in vivo by the fluorescence of other endogenous molecules. Thus, the background may exceed the signal by up to two orders of magnitude in such an environment (Parker 1987). The central problem is to extract the weak signal from the much larger background fluorescence. This can be accomplished since the signal and background emissions do not occur simultaneously. Appearance of the sensitizer infrared fluorescence is virtually instantaneous, i.e., of the order of nanoseconds, while the $^1\text{O}_2$ phosphorescence is delayed by microseconds following optical excitation. The delay is due to the fact that $^1\text{O}_2$ is formed through a collision of $^3\text{O}_2$ with T_1 . Following initial excitation it takes some time before this collision occurs. The time lag is a function of: (i) the $^3\text{O}_2$ diffusion rate in the particular solvent and (ii) the ambient $^3\text{O}_2$ concentration (Parker 1987). Some solvents, like methanol, ethanol and acetone, which have high oxygen solubility and diffusion

rates have triplet energy transfer times in the range of 0.20-0.30 μ s (Parker 1987). The transfer times will be longer in water (2-3 μ s) due to a higher solvent viscosity (Parker 1987) and lower oxygen concentrations.

In the case of continuous wave (cw) excitation, separation of the signal from the background can be accomplished through the use of a chopping technique and a lock-in amplifier. This procedure, developed by Parker (1987), is outlined in the subsequent section.

2.2 An electro-optical system for 1O_2 detection

As previously discussed, the quenching of triplet state sensitizer by ground state molecular oxygen takes place according to



The time dependence of the triplet concentration (molecules cm^{-3}) may be expressed as

$$\frac{d[T_1]}{dt} = \mu_{ap} \bar{I}_T \psi(t) - K_T [{}^3O_2] [T_1] \quad (2)$$

where K_T is the rate constant of the triplet energy transfer reaction (cm^3 molecules $^{-1}$ s $^{-1}$), $\psi(t)$ is the fluence rate (photons cm^{-2} s $^{-1}$), μ_{ap} is the absorption coefficient of the photosensitizer (cm^{-1})

and $\bar{\phi}_T$ is the quantum yield of the triplet state of the photosensitizer. In most cases maximum values of $[^1O_2]$ are much smaller than $[^3O_2]$, i.e., $[^3O_2]$ is constant and to a good approximation

$$K_T[^3O_2] = k_T \quad (3)$$

where k_T is a constant that has units of s^{-1} . Equation (2) can thus be rewritten as

$$\frac{d[T_1]}{dt} = \mu_{ap} \bar{\phi}_T \psi(t) - k_T [T_1] \quad (4)$$

The time dependence of the singlet oxygen concentration may be expressed as

$$\frac{d[^1O_2]}{dt} = \frac{\bar{\phi}_\Delta}{\bar{\phi}_T} k_T [T_1] - k_D [^1O_2] \quad (5)$$

where k_D is the rate of loss of 1O_2 due to solvent collisions and $\bar{\phi}_\Delta$ is the quantum yield of 1O_2 .

When the incident light is chopped it is desirable to filter the detector output in order to minimize the noise input to the lock-in. The filtering is done in the lock-in itself. In this situation only the fundamental of the signal is important, and it can be assumed that the excitation itself is harmonic. The first harmonic of a square wave with amplitude ψ_0 is given by $\psi(t) = 2/\pi \psi_0 e^{j\omega t}$ where $\omega = 2\pi f$ and f is the chopping

frequency. Equations (4) and (5) can thus be rewritten as

$$j\omega [T_1] = \mu_{ap} \frac{\Phi}{\tau} \psi_0 - k_T [T_1] \quad (6)$$

and

$$j\omega [{}^1O_2] = \frac{\Phi}{\tau} k_T [T_1] - k_D [{}^1O_2] \quad (7)$$

combining (6) and (7) gives

$$[{}^1O_2] = \frac{(\mu_{ap} \frac{\Phi}{\tau} \psi_0) k_T}{(j\omega + k_D)(j\omega + k_T)} \quad (8)$$

setting $k_T = (\tau_T)^{-1}$ and $k_D = (\tau_D)^{-1}$ where τ_T and τ_D are the lifetimes of T_1 and 1O_2 respectively, yields

$$[{}^1O_2] = \frac{(\mu_{ap} \frac{\Phi}{\tau} \psi_0) \tau_D}{(1 + j\omega \tau_T)(1 + j\omega \tau_D)} \quad (9)$$

The magnitude of the 1O_2 emission at 1270 nm will be proportional to $[{}^1O_2]$, and hence to ψ_0 - the exciting light intensity. The magnitude of the infrared fluorescence component will also be proportional to ψ_0 , but with a coefficient different from that specifying the 1O_2 emission. In general, the total detector output (S_T) produced by the combined emission components can be expressed as

$$S_T = A + B[{}^1O_2] \quad (10)$$

where A and B are constants which describe the detector efficiency. Equation (9) can be rewritten as

$$[{}^1\text{O}_2] = [{}^1\text{O}_2]_R - j[{}^1\text{O}_2]_I \quad (11)$$

where $[{}^1\text{O}_2]_R$ and $[{}^1\text{O}_2]_I$ represent the real and imaginary components of $[{}^1\text{O}_2]$ respectively.

Substitution of (11) into (10) yields

$$S_T = A + B[{}^1\text{O}_2]_R - jB[{}^1\text{O}_2]_I \quad (12)$$

The component of the detector output in-phase with the incident chopped radiation is thus $A + B[{}^1\text{O}_2]_R$, while the magnitude of the out of phase or negative quadrature component is

$$S_Q = B[{}^1\text{O}_2]_I \quad (13)$$

The in-phase component is thus an admixture of the sensitizer infrared fluorescence and the real component of the $[{}^1\text{O}_2]$ emission, while the negative quadrature component depends **ONLY** on the ${}^1\text{O}_2$ emission. It is this difference that allows separation of the ${}^1\text{O}_2$ emission from the much larger sensitizer infrared fluorescence. This method of isolating the ${}^1\text{O}_2$ emission thus requires chopping of the incident light in order to exploit differences in the

time behaviour of the sensitizer fluorescence and 1O_2 emissions. Chopping also provides a reference signal for the lock-in amplifier. The output in-phase and quadrature components of the lock-in are relative to this reference.

Resolving equation (9) into its real and imaginary components yields

$$[{}^1O_2]_R = \frac{(\mu_{ap} \bar{I}_\Delta 2/\pi \psi_0 \tau_D) (1 - \omega^2 \tau_T \tau_D)}{(1 + \omega^2 \tau_T^2) (1 + \omega^2 \tau_D^2)} \quad (14)$$

and

$$[{}^1O_2]_I = \frac{(\mu_{ap} \bar{I}_\Delta 2/\pi \psi_0 \tau_D) (\tau_T + \tau_D) \omega}{(1 + \omega^2 \tau_T^2) (1 + \omega^2 \tau_D^2)} \quad (15)$$

From equations (13) and (15), the quadrature signal $S_q(\underline{r}, \omega)$ due to a small volume element of the sample dV at \underline{r} is thus given by

$$S_q(\underline{r}, \omega) = B(\underline{r}, \omega) 2/\pi \psi_0(\underline{r}) \mu_{ap}(\underline{r}) \bar{I}_\Delta P_{kin} dV \quad (16)$$

where $2/\pi \psi_0(\underline{r})$ is the amplitude of the local harmonic photon fluence rate, $\mu_{ap}(\underline{r})$ is the local photosensitizer absorption coefficient and

$$P_{kin} = \frac{\tau_D \omega (\tau_T + \tau_D)}{(1 + \omega^2 \tau_T^2) (1 + \omega^2 \tau_D^2)} \quad (17)$$

The total quadrature signal measured by the detector will be the volume integral of equation (16) over the entire sample.

For the geometry used in the in vivo case (Figure 3.7) the volume integral can be evaluated if some simple assumptions are made. Since the incident beam is a small circle it can be assumed that $\psi_0(\underline{r}) = 0$ outside the beam and that, inside the beam

$$\psi_0(\underline{r}) = \psi_0(\rho, z) = \psi_0 e^{-\mu_{ex}z} \quad (18)$$

where ρ and z are the radial and depth co-ordinates respectively. The attenuation coefficient, μ_{ex} , describes the exponential fall-off of the excitation fluence in the sample. For non-turbid samples $\mu_{ex} = \mu_{ap}$, but for turbid samples such as tissue, μ_{ex} depends on the absorption and scattering coefficients. For the wavelength used here, a good approximation (Wilson and Patterson 1986) is $\mu_{ex} = 5 \text{ cm}^{-1}$.

Since a small beam is used it can be assumed that the spatial variation of $B(\underline{r}, \omega)$ is due only to the attenuation of the emitted 1270 nm light so that

$$B(\underline{r}, \omega) = B(\omega)e^{-\mu_{1270}z} \quad (19)$$

where μ_{1270} is the attenuation coefficient for 1O_2 luminescence. In aqueous samples and tissue μ_{1270} is approximately 1 and 5 cm^{-1} respectively (Patterson et al. 1988). With the assumptions of equations (18) and (19) and the further assumption that the photosensitizer is uniformly distributed, i.e., $\mu_{ap}(\underline{r}) = \mu_{ap}$, equation (16) becomes

$$S_q(\underline{r}, \omega) = B(\omega) e^{-\mu_{1270}z} \frac{2}{\pi} \psi_0 e^{-\mu_{ex}z} \mu_{ap} \bar{\Phi}_\Delta P_{kin} dV$$

for \underline{r} within the beam and $S_q(\underline{r}, \omega) = 0$ for \underline{r} outside the beam. If the sample thickness is t , the volume integral over the sample yields the total quadrature signal

$$S_q(\omega) = B(\omega) \frac{2}{\pi} \psi_0 A \mu_{ap} \bar{\Phi}_\Delta \frac{1 - \exp[-(\mu_{1270} + \mu_{ex})t]}{\mu_{1270} + \mu_{ex}} P_{kin}$$

where A is the incident beam area (0.2 cm^2 in these experiments). In subsequent sections equation (21) will be used to calculate the system sensitivity and to place lower limits on 1O_2 lifetimes in vivo.

Strictly speaking, equation (21) is only valid for the in vivo geometry used in this work (see section 3.2.3). A simple modification, however, yields an expression which can be used for the in vitro geometry as described in Chapter 3 (Figure 3.5). Thus, for the in vitro experiments,

the quadrature signal is given by

$$S_q(\omega) = B(\omega) \frac{2}{\pi} \psi_0 A \mu_{ap} \Phi_{\Delta} e^{-\mu_{1270} z} e^{-\mu_{ex} x} P_{kin} \quad (22)$$

where z and x are the distances travelled by the emitted and exciting light in solution.

If plotted as a function of angular frequency (ω), $[^1O_2]_I$ exhibits a maximum at

$$\omega_m = \left[\frac{2}{(1 + 3\eta^2)^{0.5} + 1} \right]^{0.5} (\tau_T^2 + \tau_D^2)^{-0.5} \quad (23)$$

where

$$\eta = \frac{2\tau_T \tau_D}{(\tau_T^2 + \tau_D^2)} \quad (24)$$

and the magnitude of the frequency for maximum quadrature is

$$f_m = \frac{\omega_m}{2} \quad (25)$$

For media of biological interest, τ_T and τ_D are typically of the order of microseconds which means that f_m is of the order of kHz. Such high chopping rates cannot be obtained through the use of ordinary electromechanical choppers, thus necessitating the use of an acousto-optic modulator in order to maximize the quadrature component.

CHAPTER 3

MATERIALS AND METHODS

3.1 Instrumentation

3.1.1 Description of system

A schematic diagram of the system used in this work is shown in Figure 3.1. Sensitizer excitation was accomplished through the use of a Cooper Medical Model 770 laser system consisting of two lasers. A Lexel Corp. Model 98 OEM argon ion laser pumps a Model 600 dye laser operating with dicyanomethylene (DCM) as the active dye. The argon-to-dye conversion efficiency is approximately 20 %, thus at maximum argon power (7 W) the dye output is ca. 1.4 W. Rarely, if ever, is this theoretical maximum achieved. It may be approached at the beginning of the argon tube lifetime, however, there is a rapid drop in dye power following even a few hours of use. In the interest of maintaining a stable dye output, the dye power was almost always kept below 500 mW. Wavelength selection (600-670nm) was accomplished through the use of a single element birefringent plate. The dye laser output was modulated by an Intra Action Corp. Model ADM-40 acousto-optic modulator (AOM) actuated by an Intra Action Model DE-40 VCO deflector driver. Modulation input to the driver was supplied in the

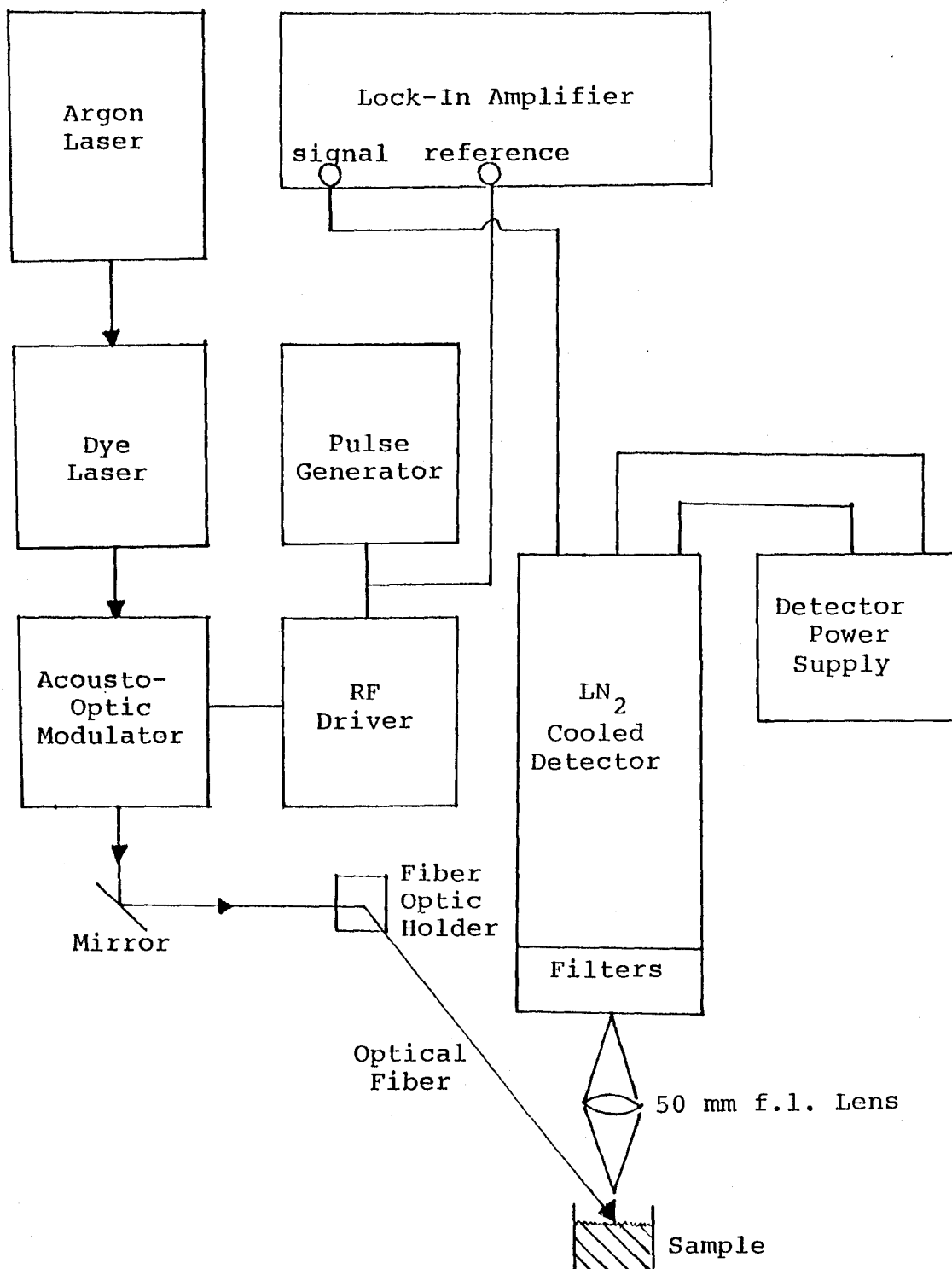
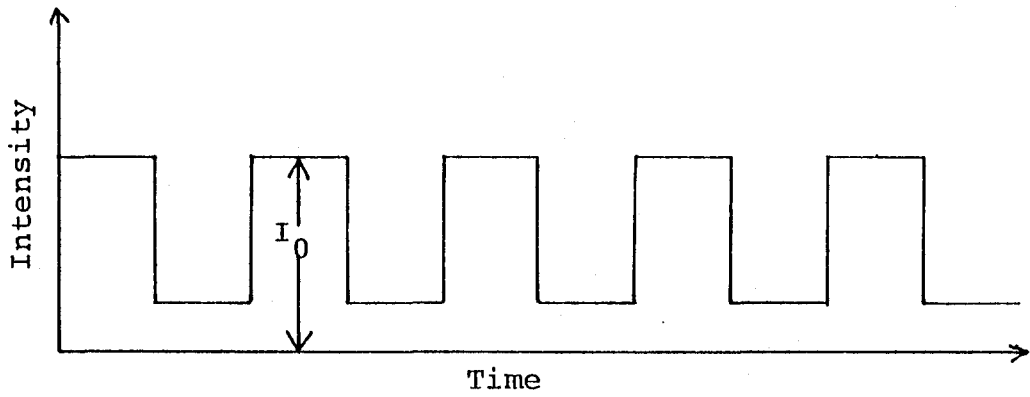


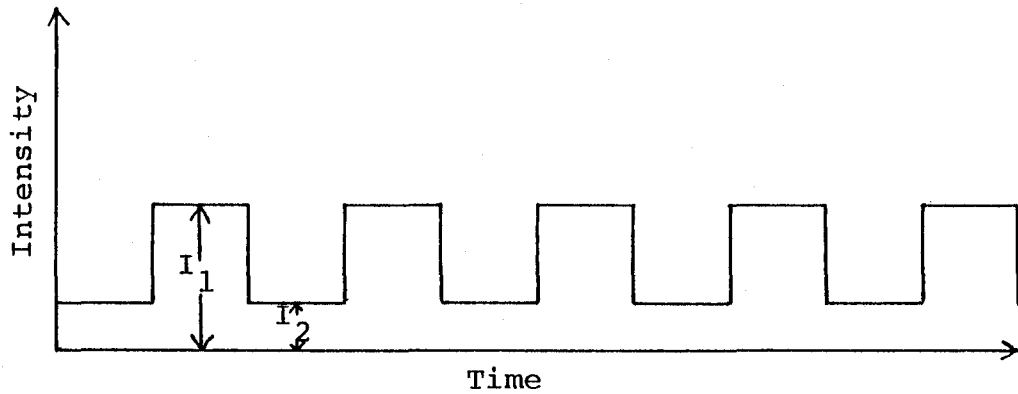
Figure 3.1 System schematic.

form of a square wave from a Wavetek Model 191 pulse/function generator.

The ADM-40 is a solid state acousto-optic light deflector-modulator made from high quality flint glass as the interaction medium with epoxy bonded lead zirconate titanate piezoelectric transducers for generating acoustic waves. In this work the ADM-40 was used as an intensity modulator, i.e., the RF input frequency was held constant while varying the signal amplitude to produce intensity modulation of the beam. Light entering the device is diffracted by the acoustic waves - a phenomenon known as Brillouin scattering. The angle of diffraction depends on the frequency of the incident light, the sound velocity and the frequency of the sound waves, i.e., the RF input frequency. For this particular device the diffraction angle at 633 nm and 40 MHz is quoted at 6.47 mrad (Intra Action Corp 1987). The diffraction efficiency, defined as the percentage of incident light diffracted into the first main order depends on the beam diameter, on the RF input frequency (and power) and on the angle between the incident light beam and the sound field. From Figure 3.2 the diffraction efficiency is given by $I_1/I_0 \times 100 \%$. The extinction ratio, defined as the ratio of on/off beam intensity in the first order (I_1/I_2 in Figure 3.2) also depends on the above four parameters. Empirically, it was



Zeroth Order



First Order

Figure 3.2 Illustrations of diffraction efficiency and extinction ratio.

found that the diffraction efficiency and the extinction ratio were simultaneously optimized. Optimization of the extinction ratio involved setting the RF input frequency to 40 MHz (according to manufacturer's suggestion) and reducing the size of the beam emerging from the laser aperture. Beam reduction was necessary since it was discovered that the beam diameter exceeded the entrance slit of the ADM-40. A special lens mount was thus constructed and fitted into the laser beam port. A 50 mm f.l. (25 mm dia.) lens was fixed to the mount producing a beam at the ADM-40 entrance window of between 1.5 and 2.0 mm dia. The size and quality of the beam were usually altered following periods of laser repair. On most occasions however, the beam diameter was approximately 2.0 mm.

The diffraction efficiency (2.0 mm beam), measured on several different occasions, was found to vary between 50 and 60 % - well short of the 85 % optimum quoted value (Intra Action Corp 1987). On the rare occasion that a 1.5 mm high quality beam was obtained, the diffraction efficiency was approximately 90 %. An extinction ratio of better than 100:1 was observed with the diffracted 2.0 mm beam on numerous occasions. Again, this is well short of the optimum quoted value of 1000:1 (Intra Action Corp. 1987). Extinction ratios of 1000:1 were obtained with the

1.5 mm high quality beams.

The on/off diffraction pattern emerging from the ADM-40 was reflected through 90° using an adjustable front surface mirror positioned at 45° to the laser axis. The first order diffraction maximum was then focused into a 0.4 mm optic fiber by a 25 mm f.l. (12.7 mm dia.) lens. Discrimination of diffraction orders was accomplished through the design of a special lens mount. The lens was positioned in the mount and a removable circular steel plate with a 2 mm central aperture was positioned in front of the lens. The necessary modulator-to-aperture distance was determined using geometrical considerations given a 6.47 mrad diffraction angle and a 2 mm spacing between adjacent maxima. Design constraints (see below) dictated a maximum spacing of 2 mm which was found to be adequate for this work.

The fiber was held in place using an adjustable fiber holder which could be moved in three dimensions. The fiber holder, lens mount, mirror and acousto-optic modulator were all fastened to a steel plate which in turn was fixed onto the laser cabinet such that the above mentioned components were at beam level (Figure 3.3). The plate had to be designed in such a way that it could easily be removed during periods of laser repair. Since the laser is located perilously close to the laboratory door and the

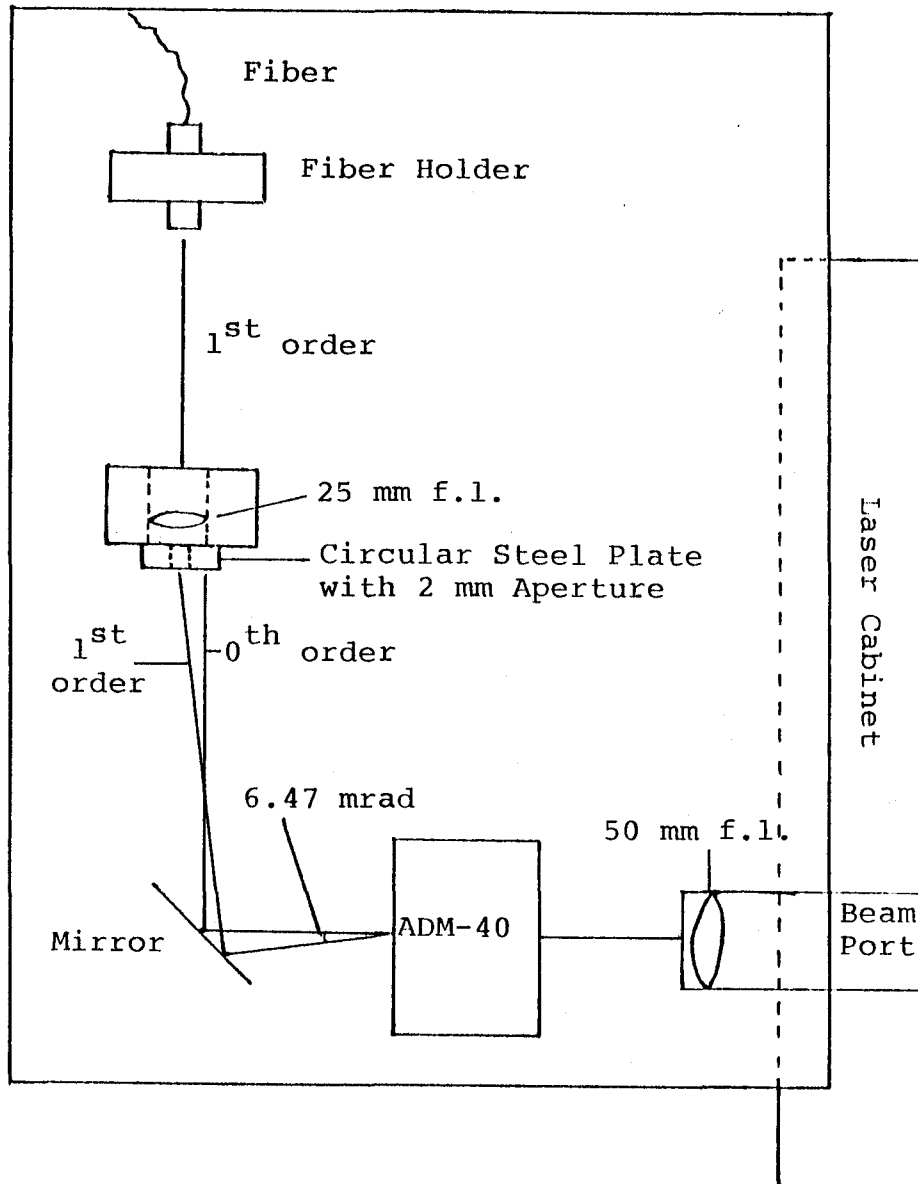


Figure 3.3 Overhead view of ADM assembly plate.

steel plate was at head level, it had to be designed as small as possible for safety reasons.

The distal end of the optical fiber was inserted into a small steel cylindrical lens holder containing a 15 mm f.l. (12.7 mm dia.) lens. The fiber was moved along the long axis of the cylinder until the emerging beam (ca. 5 mm dia.) was in focus. At that point the fiber was fixed in place by adjusting a set screw. For sample irradiation, the cylinder was held in place by an adjustable clamp fastened to a retort stand. The sample was placed on or in a specially designed cuvette holder - a circular steel column with a depression at the top. In order to reduce scattered light at the detector, a square shield with an 8 mm circular aperture was attached to the cuvette holder parallel to the incident beam. The emitted signal thus had to pass through this aperture in order to be detected.

The optical light collection system consisted of a 50 mm f.l. (50.8 mm dia.) double convex lens used to direct the light emitted from the irradiated sample through the optical filtering system and into the detector. The lens was mounted in a specially designed holder which had three degrees of freedom. The lens position with respect to the sample and the detector was determined by trial and error. Optimum signal input to the detector occurred at a lens-to-cuvette distance of approximately 2 f.l.s. (85 cm)

and a lens-to-detector distance of 2 f.l.s. (100 cm).

The liquid-nitrogen-cooled germanium detector was obtained from North Coast Optical Systems and Sensors (Model E0-817S) with power provided by a Model 823A supply adjusted to 300 V. The minimum detector time constant, as determined from the detector response to background events, was found to be 30.8 μ s and the quoted noise equivalent power (NEP) at 1400 nm using a chopping frequency of 100 Hz and a detection bandwidth of 1 Hz was approximately 2.0×10^{-14} W Hz^{-1/2} (North Coast Optical Systems and Sensors 1987). The cylindrical detector was immobilized by placing it in a custom designed cradle which was fastened to two carriages. The cuvette holder and lens holder were also fastened onto carriages which could slide freely on an optical bench. Distances between the three components could thus be varied with a minimum of effort. Once the proper distances had been found, the carriages were locked in place.

Optical input to the detector was filtered using one of three bandpass filters. Two of the filters lie completely outside the ¹O₂ emission band which is centered at 1270 nm (Whitlow and Findlay 1966). These filters exhibit maximum transmission at 1201 nm (54%) and 1303 nm (44%) with widths (FWHM) of 9.4 and 8.5 nm respectively. The third filter, centered at 1272 nm (44%

transmission) with a FWHM of 17.9 nm, significantly overlaps the region of $^{1}O_2$ emission, but not the other two filters. The relationship of the three pass bands to the $^{1}O_2$ emission spectrum determined by Whitlow and Findlay (1966) is shown in Figure 3.4.

The filters were arranged in a sliding mechanism such that at any given time only one of the filters was positioned in front of the detector window. Filter selection simply involved pushing or pulling the sliding mechanism until the desired filter was positioned in front of the detector window. The sliding mechanism was incorporated into a sleeve which was designed to fit snugly over the detector head. A permanent long-pass infrared filter (92 % transmission between 1200 and 1300 nm) was placed in front of the sliding mechanism in order to reduce the scattered light reaching the detector (Figure 3.4).

Separation of the in-phase and quadrature components from the total detector output was accomplished through the use of a Stanford Research Systems Model SR 510 lock-in amplifier. The methods by which this separation was accomplished will be outlined in a later section.

3.1.2 Optimization of optical output and detector input

In all cases, prior to each experiment, the optical output at the end of the fiber was maximized by adjusting some or all of the components on the AOM assembly plate. On

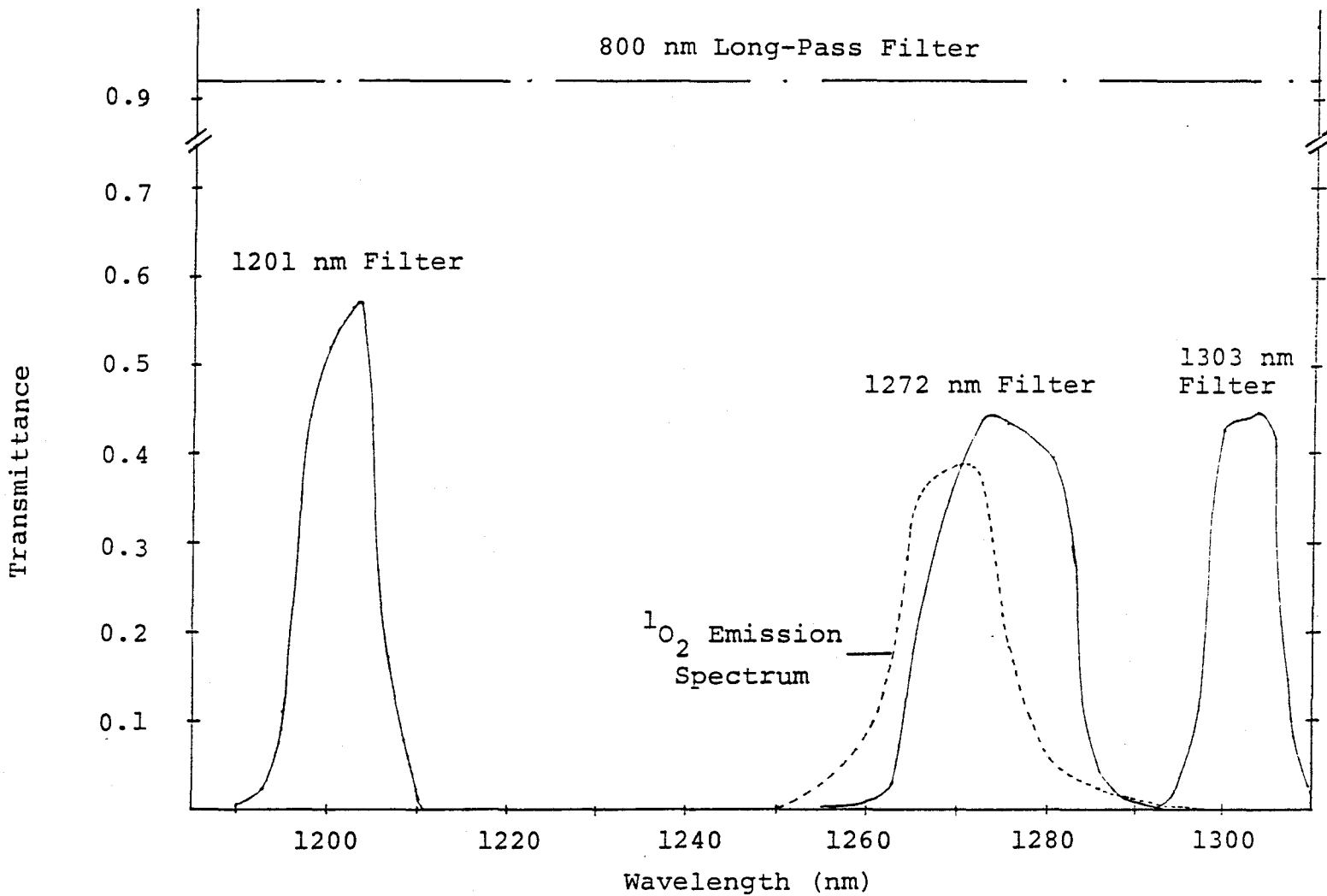


Figure 3.4 Sketch of filter pass bands and $^1\text{O}_2$ emission spectrum.

numerous occasions the dye laser power was too low to carry out useful experiments. The problem was usually remedied by alignment of the laser optics. However, this usually produced a large change in the position of the emerging beam. In such cases the beam had to be "walked" onto the entrance slit of the ADM-40 using the position controls on the laser beam port. Having ensured that the beam entered the center of the ADM-40 entrance slit, the mirror was rotated out of the optical path so that the diffraction pattern appeared on the laboratory wall a few meters away. The three position settings on the ADM-40 were then adjusted in order to maximize the extinction ratio and diffraction efficiency. At this time the RF signal amplitude was also checked to ensure that it was set at the proper level for optimization of these parameters. An Ophir Model DG laser power/energy meter was used to determine the extinction ratio and diffraction efficiency.

The mirror was then rotated back into place and adjusted in such a way as to allow the first order maximum through the aperture (and through the lens) while rejecting as much of the zeroeth order as possible. The fiber holder was removed and replaced with the Ophir Model DG which allowed an evaluation of the extinction ratio of the first order diffraction maximum. When the optimum ratio had been obtained, the fiber holder was returned to its normal

position and the fiber was inserted into the holder. The position of the fiber was then adjusted for maximum output by varying the three position controls on the fiber holder. The output was monitored at the other end of the fiber by the Ophir Model DG.

The procedures described above for optimizing the optical output were quite time consuming. Fortunately, they were only required on those occasions where the laser optics had to be readjusted. In the vast majority of cases optimization of the output was accomplished simply by fine tuning the ADM-40 Bragg angle and monitoring the output at the end of the fiber. Fine tuning was required since it was discovered that the position settings on the ADM-40 drifted slightly with time.

In the majority of cases, due to poor beam quality, the optical output at the end of the cylindrical lens holder was only 10-15 % of the beam emerging from the laser aperture, i.e., 85-90 % of the beam was lost in passing through the optical system. This is far greater than expected due to losses at the various interfaces. For example, each of the three lenses in the system transmit 92 % of the incident light while the front surface mirror reflects approximately 100 %. Transmission through the ADM-40 is also 100 % due to its optically coated entrance and exit windows. Transmission through the optical fiber is

approximately 90 %. Thus for an incident beam of 100 mW and a 55 % diffraction efficiency, the theoretical output at the cylindrical lens holder should be ca. 38.5 mW. However, the observed output (12 mW) was a factor of three lower than expected. This large discrepancy was attributed to losses at the ADM-40 and the lens holder in front of the fiber. Due to the large beam size (2.0 mm dia.), a small fraction of the beam hit the face of the ADM-40 and was lost. Losses at the lens holder were due to the fact that the first order diffraction maximum did not pass cleanly through the 2.0 mm aperture in front of the lens. It was discovered that this maximum had to be shifted slightly from the center of the aperture in order to minimize the light contribution from the zeroeth order. Failure to do this resulted in a poor extinction ratio. On the few occasions where a high quality 1.5 mm dia. beam was obtained, only 50 % (approx.) of the beam was lost in passing through the electro-optical system. Using the same transmission values as above for the various interfaces, the theoretical output at the cylindrical lens holder for a 100 mW incident beam and a 91 % diffraction efficiency should be approximately 127 mW. The actual output was 98 mW. In this case, due to the small beam size there was no loss at the ADM-40. The entire loss thus occurred at the lens holder due to optimization of the extinction ratio as

described above.

Having optimized the optical output, the lens holder containing the fiber end was placed in a three pronged adjustable clamp which was attached to a retort stand. The retort stand was placed beside the optical bench such that the end of the cylinder was approximately 23 mm from the sample. The clamp was raised such that the beam was parallel to the center of the cuvette shield aperture. The detector was then placed in its cradle, the appropriate electrical connections made and the cradle pushed along the optical bench until the distance from the center of the 50 mm f.l. lens to the active volume of the detector was 2 f.l.s. The sample was placed in or on the cuvette holder and measurements using the lock-in amplifier were initiated.

3.1.3 Lock-in detection procedure

Extraction of the $^1\text{O}_2$ emission from the sensitizer infrared fluorescence background involved adjusting the lock-in phase to produce a zero-quadrature reading using the 1201 nm filter. A true zero reading was never obtained due to random fluctuations associated with detector noise. This was especially true at low frequencies where the noise was quite substantial. The in-phase component was found by altering the phase by 90° . Since the $^1\text{O}_2$ luminescence is negligible at 1201 nm (Whitlow and Findlay 1966), the signal appearing at the lock-in

input will be due only to infrared fluorescence thus providing a valid reference. With both pre and post filters set at one second, it can be shown that the signal reaches 1 % of its final value within 7 seconds. Thus, before taking any in-phase readings, a waiting period of ca. 10 seconds was observed from the time of the phase change. Following the waiting period, five readings were taken at approximately two second intervals (the time it took to record a reading) and the mean and standard deviation were evaluated. This procedure was repeated following each filter and 90° phase change.

Having recorded the 1201 nm in-phase component, the 1272 nm filter was moved in front of the detector window. Using the optimal setting found at 1201 nm, the in-phase component was recorded. In this case, the in-phase component was a combination of the 1O_2 emission and the sensitizer infrared fluorescence since the 1O_2 emission peak occurs at 1270 nm (Whitlow and Findlay 1966). The phase was then changed by 90° and the quadrature component recorded. This signal was entirely due to the 1O_2 emission. The 1272 nm filter was then replaced by the 1303 nm filter and the quadrature component recorded. The phase was then changed by 90° in order to record the in-phase component. As was the case with the 1201 nm filter, the signal should be composed entirely of

sensitizer infrared fluorescence since, according to Whitlow and Findlay (1966), the $^1\text{O}_2$ luminescence is also negligible at 1303 nm. The purpose of this filter was thus to verify the $^1\text{O}_2$ emission spectrum as determined by Whitlow and Findlay (1966).

Phase drift was checked for during most trials by returning to the 1201 nm quadrature component after having recorded the 1303 nm in-phase component. If the quadrature component failed to return to the initially set zero, the trial was repeated. On several occasions phase stability was monitored during $90^\circ - 90^\circ$ shifts (using one filter) and found to be satisfactory.

3.2 Sample preparation and experimental set-up

3.2.1 Solution experiments

All solutions were irradiated in a quartz cuvette (1 cm x 1 cm x 4.5 cm) transmitting between 320 and 2500 nm. The cuvette was placed in the holder such that one side was perpendicular to the incident beam (Figure 3.5). The excitation wavelength was chosen to match the absorption peak of the given photosensitizer. The 2.5 mg ml^{-1} stock solution of PFII in isotonic saline solution was supplied by Photomedica, Inc. (Raritan, New Jersey). AlSPc was received in powder form from Porphyrin Products, Inc. (Logan, Utah). A 2.5 mg ml^{-1} stock solution was prepared

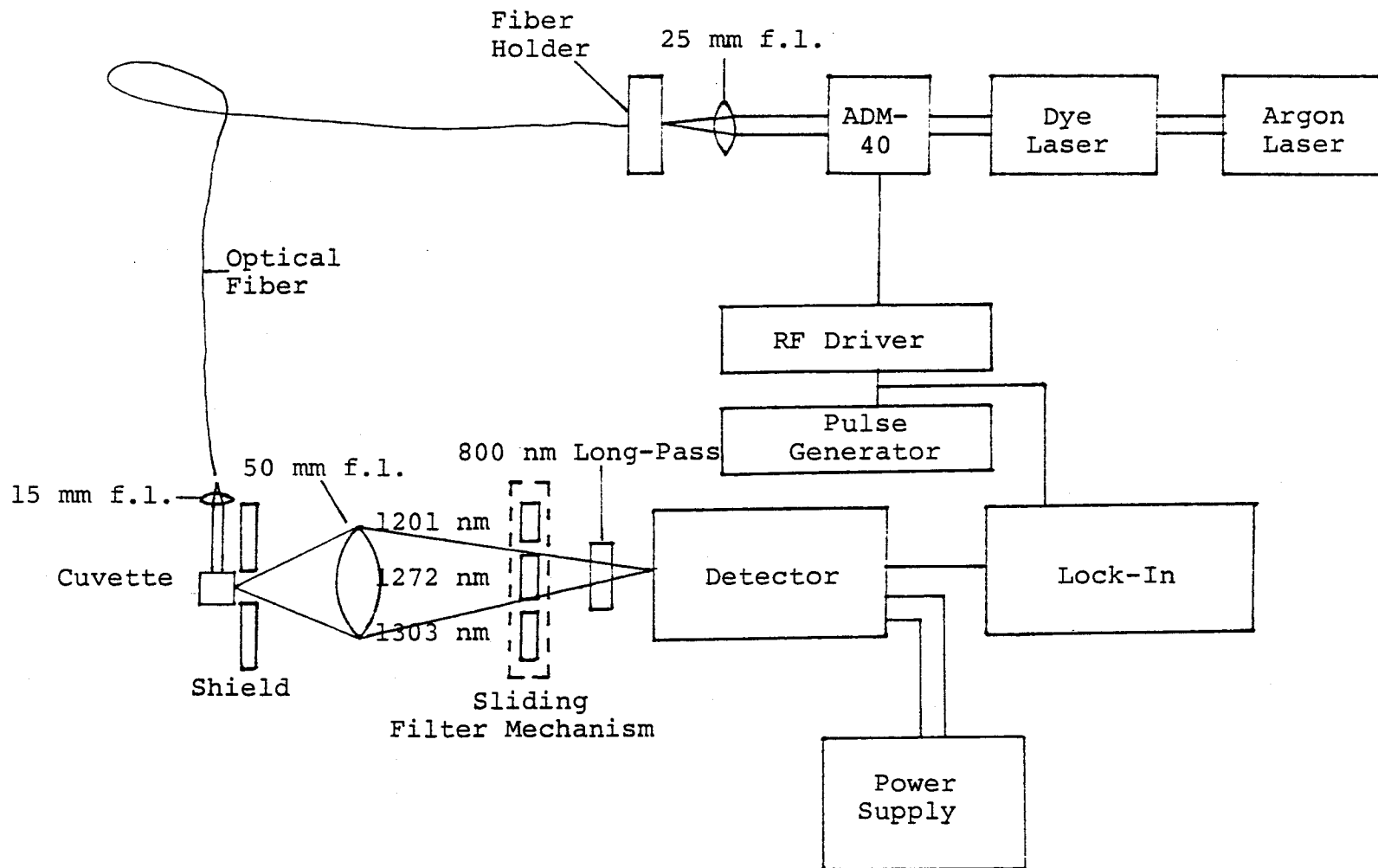


Figure 3.5 In vitro geometry.

by dissolving the powder in physiological saline (0.9% NaCl in H₂O). ACS Spectro Grade methanol was obtained from Caledon Laboratories Ltd (Caledon, Ontario). Absorption spectra of AlSPc and PFII, both in MeOH at a concentration of 50 $\mu\text{g ml}^{-1}$, are shown in figures 3.6a and b. The AlSPc spectrum was actually determined at a concentration of 10 $\mu\text{g ml}^{-1}$ since the spectrophotometer could not reliably handle concentrations above this value. The plotted values have thus been multiplied by a factor of five. From figures 3.6a and b the peak excitation wavelengths of AlSPc and PFII were found to be 624 and 675 nm respectively. However, the AlSPc excitation wavelength was set at 670 nm - the maximum wavelength achievable with the dye laser.

The irradiation procedures described at the beginning of this section were also applied to the aqueous and protein containing solutions. However, prior to irradiation, the detector input was maximized by examining its output as a function of lens (50 mm f.l.) distance using a standard solution of 50 $\mu\text{g ml}^{-1}$ PF II in MeOH. Non sterile phosphate buffered saline (PBS) at a pH of 7.2 was prepared in the laboratory while fetal calf serum (FCS) was supplied by Gibco Laboratories (Grand Island, New York).

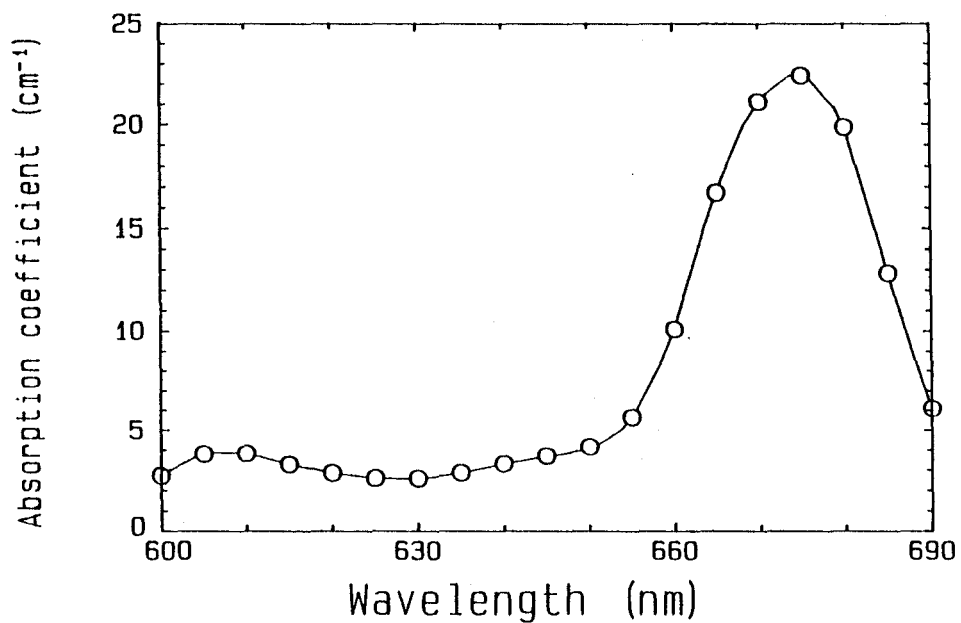


Figure 3.6a Absorption spectrum of AlSPc in MeOH ($50 \mu\text{g ml}^{-1}$).

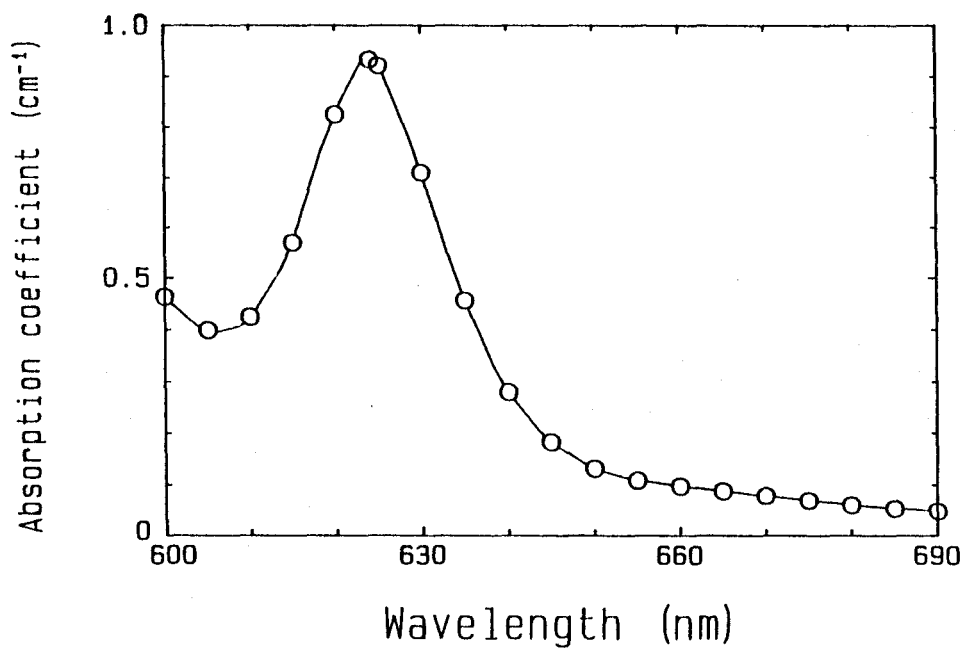


Figure 3.6b Absorption spectrum of PFII in MeOH ($50 \mu\text{g ml}^{-1}$).

3.2.2 Cell suspension experiments

The P388 cell line used was derived from a lymphoid neoplasm originating in a DBA/2 mouse. In vitro, the line exhibits a doubling time of 10-12 hours and grows as a stationary suspension culture. The P388 cells were incubated at a concentration of 2×10^6 viable cells per ml in medium (Opti-MEM I supplied by Gibco Laboratories) and FCS. The cells were incubated in the dark at 37° C and 5 % CO₂ with either PFII or AlSPc at a concentration of 50 $\mu\text{g ml}^{-1}$. Following the incubation period, in all but one case, the cells were spun down in a centrifuge at 1000 rpm for five minutes and then washed in PBS (1000 rpm for five minutes). The cells were spun down in order to concentrate them in pellet form thus allowing for easy removal of the incubation medium. The purpose of the PBS wash was to remove any excess drug not bound to the cells. The spinning down and washing procedures ensured that the photosensitizer was bound only to the cells and not present in the medium. In the one instance where these procedures were not performed, the drug was present in both medium and cells. Following the PBS wash, the cells were either resuspended in PBS or in medium and FCS. A pre-irradiation cell count was performed using a haemocytometer and the cell concentration was set to the desired value. The purpose of the cell count was to determine how many cells

were lost due to the incubation procedure, thus allowing an assessment of the treatment procedure. In this manner any differences in photosensitizer dark cytotoxicity were eliminated.

Prior to cell irradiation, the standard solution was again used to optimize the detector input. The cell suspension was pipetted from a test tube into a cuvette and the height of the cuvette holder adjusted such that the incident beam hit the lower portion of the cuvette. This was deemed necessary since the cells gradually settled near the bottom of the cuvette. The irradiation geometry was identical to that used in the solution experiments (Figure 3.5). Following treatment the cell cultures were tested for viability using trypan blue. The dye accumulates in the dead cells since their membranes have been damaged. The dead cells thus appear blue and can easily be distinguished from the living ones.

3.2.3 In vivo experiments

The tumour model selected for the in vivo $^{1}O_2$ measurements was the methylchlorantrene-induced fibrosarcoma (MIFS) tumour (Varani, et al. 1978) in C57/blJ6 mice (Jackson Labs). The tumour cells, which were injected into the footpad of each of the six mice used, were allowed to grow until they reached a maximum diameter of 1 cm. The average weight of the 4-6 week old male mice

was 26 gm. The mice were placed into three groups according to the level of photosensitizer received. The high level group was injected i.p. with 50 mg kg^{-1} of body weight PFII while the low level group received 10 mg kg^{-1} . The two mice in the control group were not injected with the sensitizer. The time delay between injection and irradiation was 24 hours. The laser wavelength was set at 624 nm in all cases.

Prior to irradiation, the standard solution previously described was used to maximize the detector input. During measurements the mice were anaesthetized i.p. with Somnotol (sodium pentobarbital) and placed on a lucite plate which was fastened to the top of the cuvette holder. The footpad tumour was placed as close to the shield aperture as possible. In order to minimize attenuation of the excitation and luminescence, the beam was brought in through the front of the shield aperture (Figure 3.7). Using this front surface geometry, each mouse was irradiated for ca. 30-40 min. during which they were exposed to a total surface light fluence of approximately 200 J cm^{-2} . It should be mentioned that the fingertip of a volunteer was irradiated in order to compare the fluorescence to that observed with the mice.

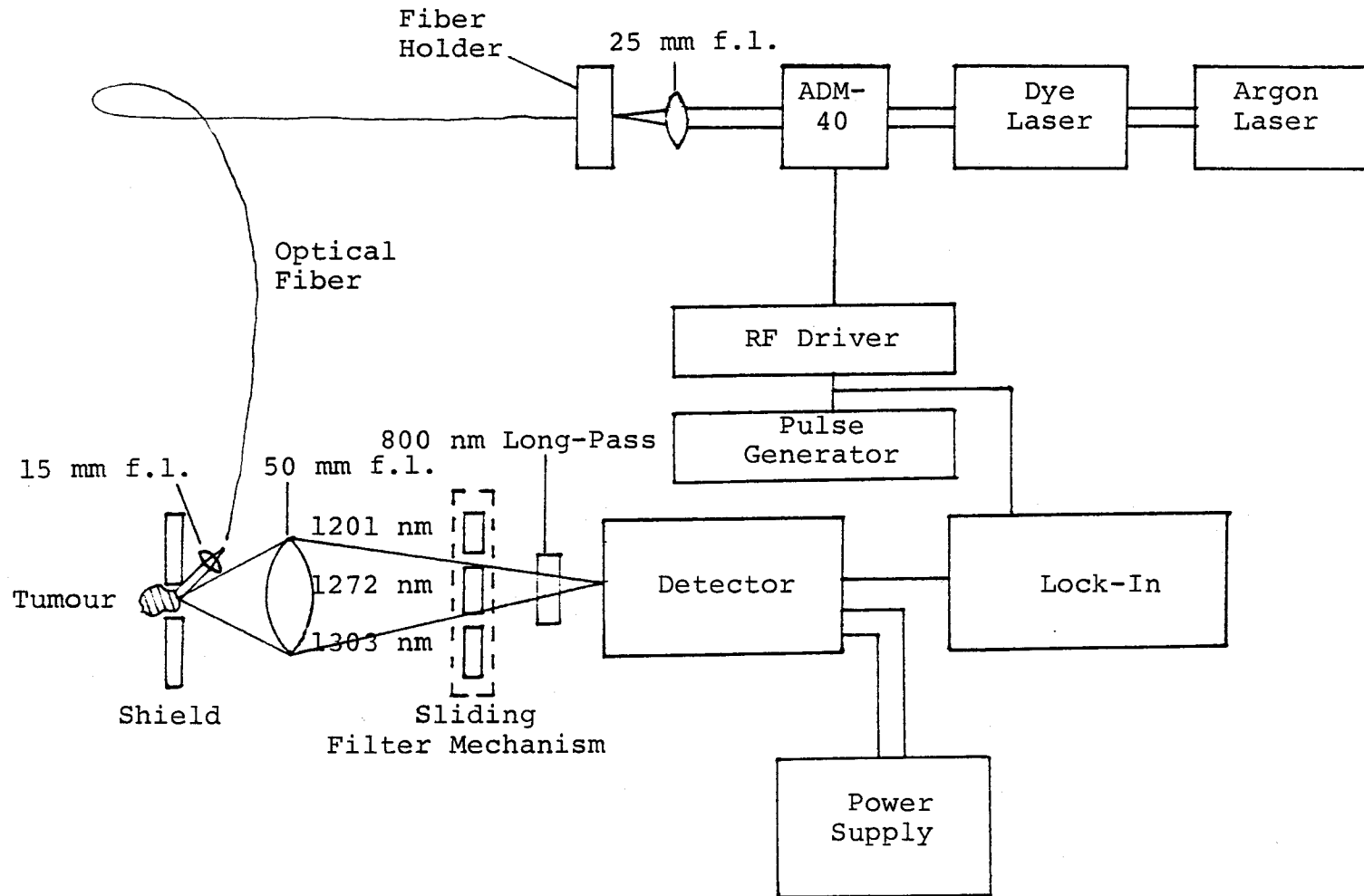


Figure 3.7 In vivo geometry.

CHAPTER 4

RESULTS AND DISCUSSION

4.1 Evaluation of the system performance

The purpose of this experiment was to measure $B(\omega)$ - the system sensitivity as a function of chopping frequency. Knowledge of $B(\omega)$ allows an evaluation of the NEP, and hence, a comparison of the detector capability to that quoted by the manufacturer. A $4 \mu\text{g ml}^{-1}$ solution of PFII was prepared and the quadrature signal was measured as a function of chopping frequency (cf Figure 4.4). From the literature $\bar{I}_\Delta = 0.25$ (Keir et al. 1987), $\tau_D = 10.4 \mu\text{s}$ (Rodgers 1985), $\tau_T = 0.25 \mu\text{s}$ (Parker 1987) and $\mu_{1270} = 0.37 \text{ cm}^{-1}$ (Morita and Nagakura 1974). At 624 nm, $\mu_{\text{ex}} = \mu_{\text{ap}} = 0.074 \text{ cm}^{-1}$ (measured) and equation (22) may be solved for $B(\omega)$. The results of this calculation are shown in Figure 4.1 along with the measured electronic rms noise. Also shown in Figure 4.1 is the theoretical response of the detector calculated from the impulse response and normalized at 2 kHz (see Appendix A for calculation). From the figure it can be seen that below approximately 10 kHz, the sensitivity falls very slowly whereas it falls essentially as $1/f$ above 10 kHz. At 1 kHz, $B(\omega) = 1.39 \times$

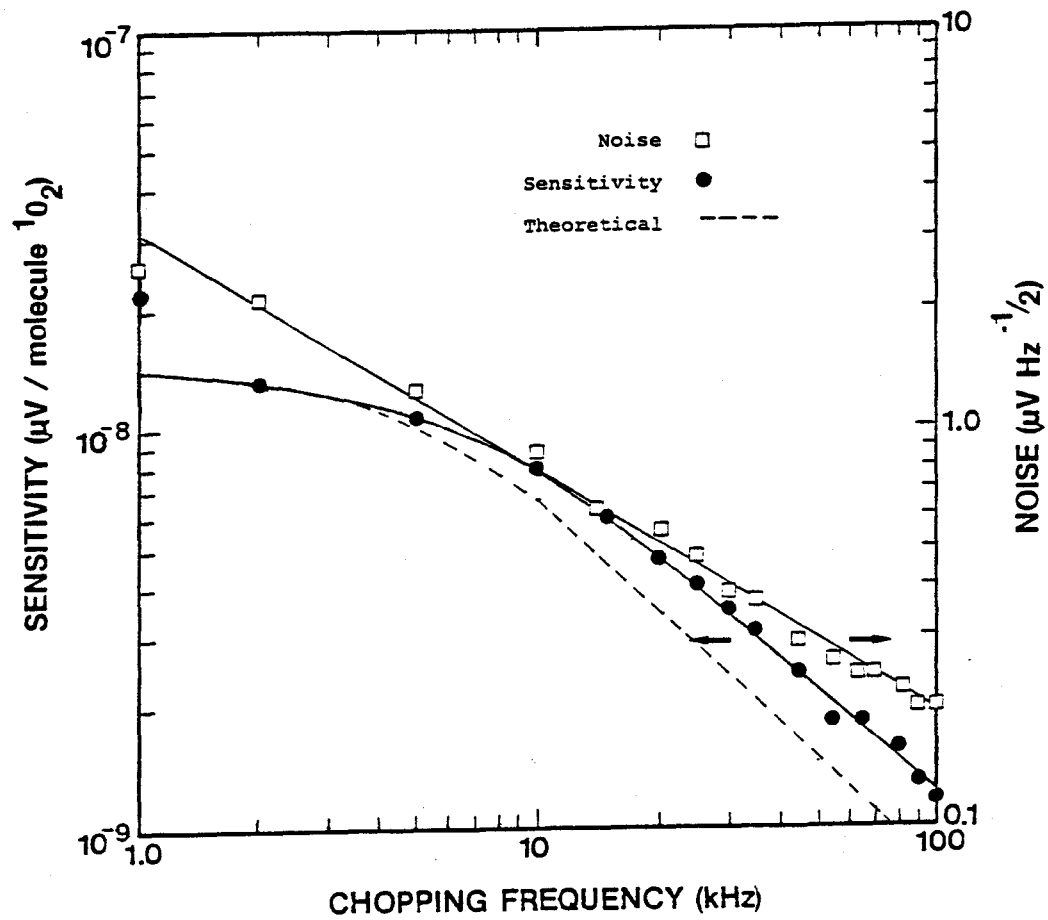


Figure 4.1 Detector sensitivity and noise versus chopping frequency.

$10^{-8} \mu\text{v molecule}^{-1}$ and the noise is approximately $3.1 \mu\text{v Hz}^{-1/2}$. It should be mentioned that, since the experimental $B(\omega)$ value at 1 kHz appears to be an outlier (Figure 4.1), the theoretical value was used. A simple calculation thus shows that, with a detection bandwidth of 1 Hz, the detection threshold is approximately 2.23×10^8 molecules.

Using the above information, it is possible to calculate the NEP of the detector. According to Parker (1987), since the average emitted power is $4 \times 10^{-20} \text{ W molecule}^{-1}$, the total emitted rms power at the detector threshold is $6.31 \times 10^{-12} \text{ W}$. Now, in order to obtain the NEP of the detector, the collection efficiency of the system must be evaluated. The 1272 nm bandpass filter transmits 44% of the incident light while approximately 28% of the light is lost in passing through the seven interfaces in front of the active volume. As previously stated, the 50.8 mm lens is located 85 mm from the shield aperture. The solid angle is thus given by

$$\frac{\pi}{4\pi} \left[\frac{25.4 \text{ mm}}{85 \text{ mm}} \right]^2 = 0.022$$

and the collection efficiency = $(0.44)(0.72)(0.022) = 6.97 \times 10^{-3}$. The power incident on the detector at the detection threshold is thus $4.4 \times 10^{-14} \text{ W}$. Since a

bandwidth of 1 Hz was used, the NEP = 4.4×10^{-14} W Hz^{-1/2}. Considering the numerous uncertainties in the calculation, this is in good agreement with the value of 3.1×10^{-14} W Hz^{-1/2} at 1272 nm obtained from the spectral response provided by the manufacturer (Figure 4.2). This leads to the conclusion that the system is functioning close to the expected noise limit. Further evidence of the correct functioning of the system is shown in the next section. Finally, Figure 4.3 (NEP versus chopping frequency) illustrates that the minimum NEP occurs around 10 kHz where a calculation similar to the one above leads to an NEP value of 1.8×10^{-14} W Hz^{-1/2}. Movement away from 10 kHz in either frequency direction results in an increase in the NEP.

4.2 Detection of ¹O₂ in solution

4.2.1 Introduction

As described in this work, one method of quantitating the biological effects due to PDT involves monitoring of the ¹O₂ emission from the tumour volume of the patient. However, before performing any biological measurements, it is imperative that the validity of the experimental procedure be established. The first step towards this goal was taken in the previous section where it was discovered that the system performed very close to

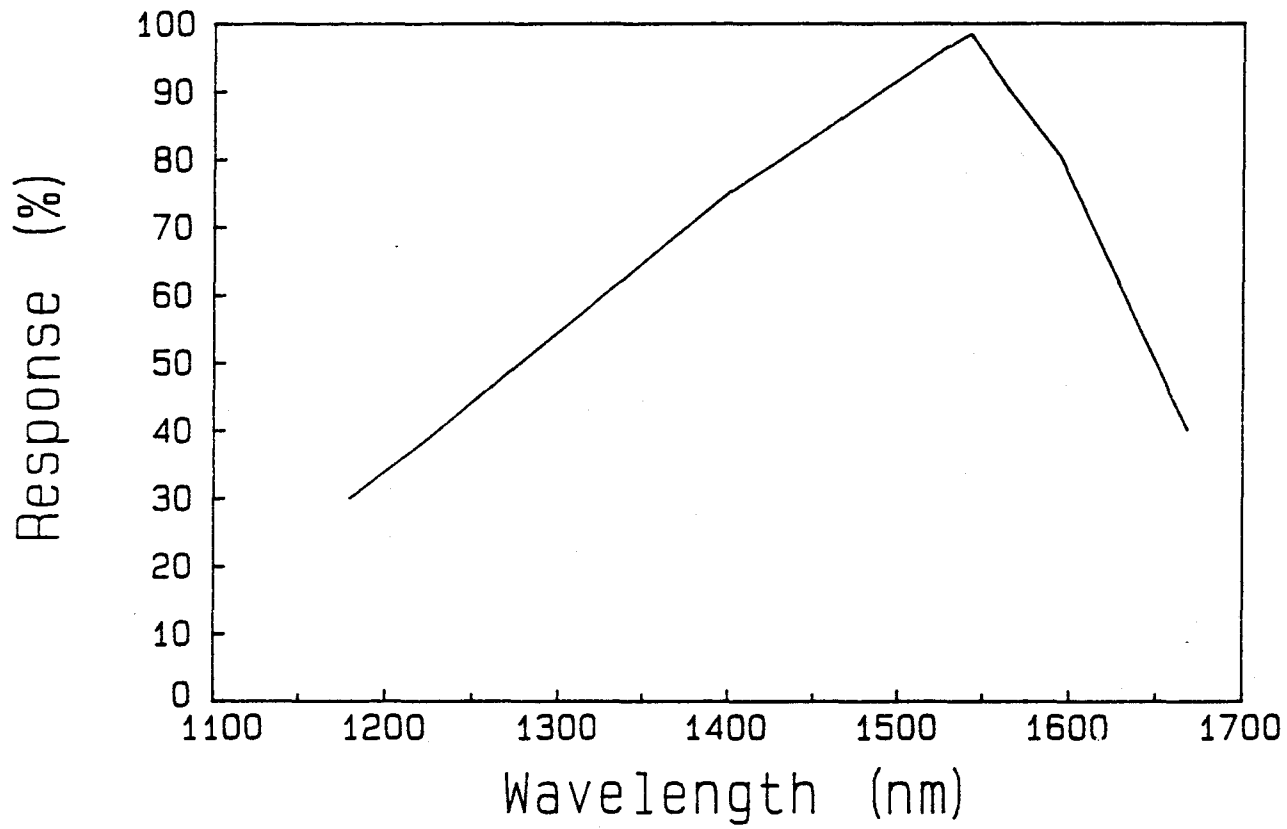


Figure 4.2 Spectral response of the E0-817S (supplied by North Coast Optical Systems and Sensors).

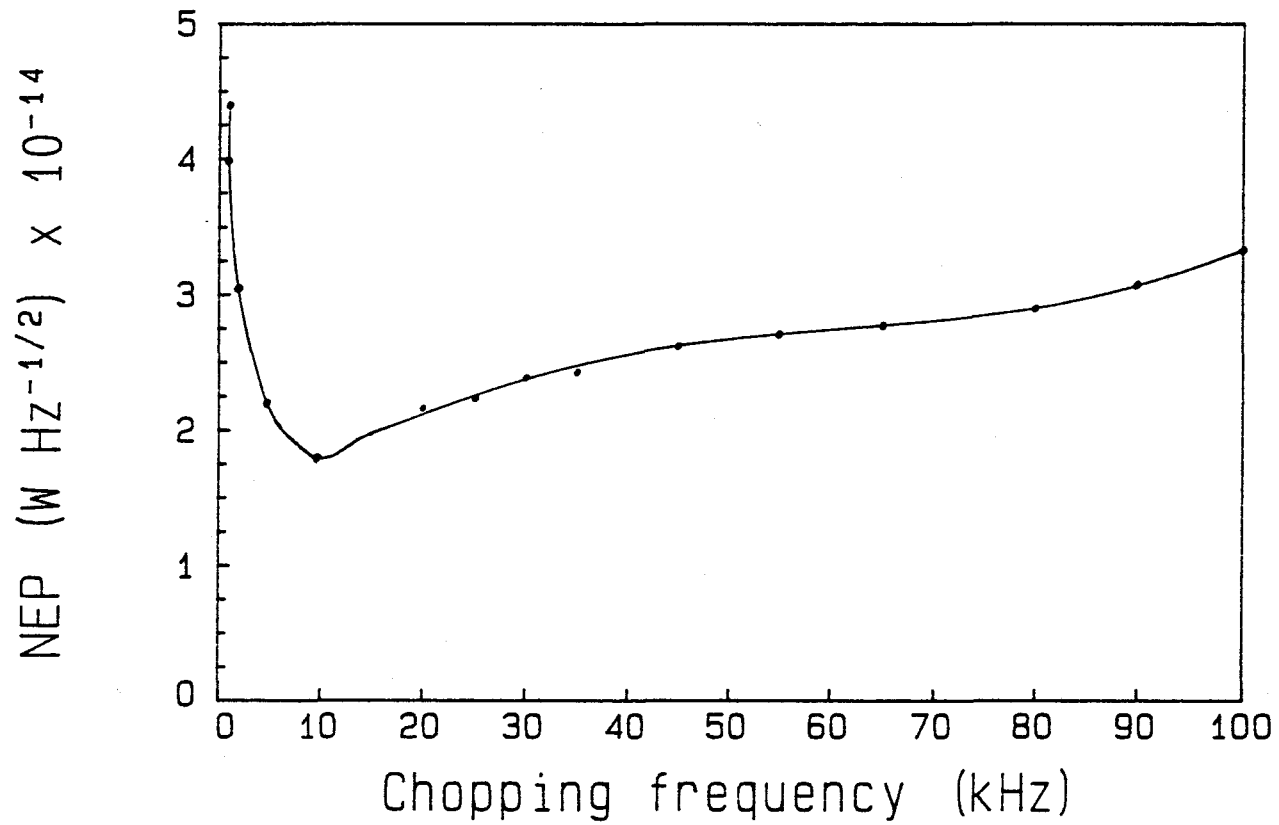


Figure 4.3 NEP versus chopping frequency.

the expected noise limit. In the series of experiments described in this section, in-phase and (negative) quadrature data were obtained as a function of chopping frequency for two different photosensitizers (PFII and AlSPc) in aqueous (PBS) and organic (MeOH) media. Since DHE (the biologically active component of PFII) is not known to form aggregates in organic solvents, it has a relatively high $^1\text{O}_2$ quantum yield (ϕ_{Δ}) in MeOH (0.25 - Keir et al. 1987). The PFII-MeOH mixture was thus expected to provide an easy test of the system's $^1\text{O}_2$ detecting capability. At the other extreme, PBS was chosen since the ϕ_{Δ} is drastically reduced in aqueous solution due to DHE aggregation (Kessel 1984). To complicate matters further, the emission intensity is reduced since, of all fundamental biological media, water exhibits the maximum $^1\text{O}_2$ quenching rate (Parker 1987). For these reasons then, it is extremely difficult to detect $^1\text{O}_2$ emissions in aqueous solutions when using photosensitizers, such as PFII, which are known to aggregate. AlSPc, on the other hand, remains monomeric in aqueous solution (Darwent et al. 1982) making detection of the $^1\text{O}_2$ emission in such an environment much easier.

4.2.2 Detection of $^1\text{O}_2$ in MeOH and PBS using PFII

Results of the in-phase and quadrature components as functions of chopping frequency using two different

concentrations (50 and 4 $\mu\text{g ml}^{-1}$) of PFII in MeOH are shown in Figure 4.4. In order to remove the wavelength dependence of the detector output, the 1272 nm data was normalized to the in-phase 1201 nm data. The shape of the curves will thus be determined by the ω , τ_T and τ_D dependent parts of equations (14) and (15). Normalization also corrects for any variations in the geometrical set up. The normalized in-phase data plotted in Figure 4.4 is thus the ratio of the in-phase component at 1272 nm to the corresponding output at 1201 nm, and the normalized quadrature data is given by the ratio of the quadrature component at 1272 nm to the in-phase component at 1201 nm. From Figure 4.4 it can be seen that there is no significant difference in the curves as a function of photosensitizer concentration. This is an interesting observation since, in an earlier experiment, it was observed that, at high PFII concentrations, the quadrature signal was not linear with concentration even when corrections were made for the greater absorption of the exciting light. This may be due to quenching of $^1\text{O}_2$ by dye molecules as found by Sinclair et al. (1987) for other photosensitizers. Such quenching would imply a reduction of τ_D and hence a change in the shape of the quadrature versus frequency curve at higher concentrations. However, as noted above, there were no significant differences in the two quadrature curves.

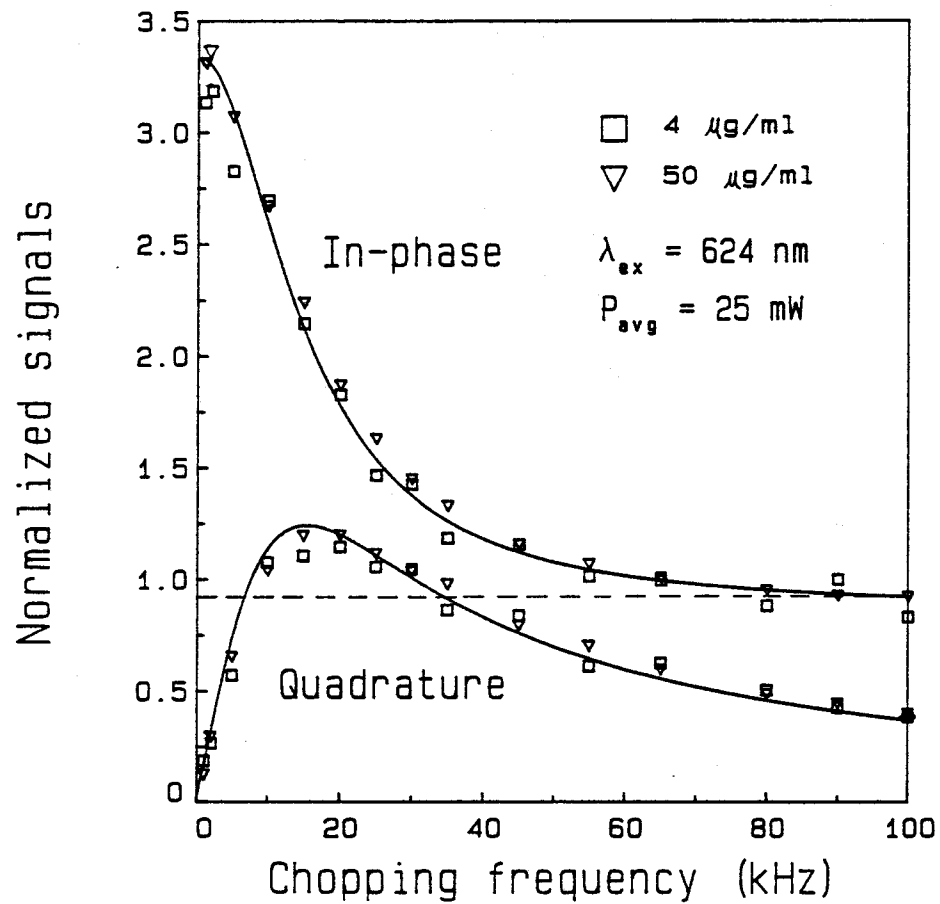


Figure 4.4 Normalized in-phase and quadrature outputs versus chopping frequency (PFII in MeOH).

The quadrature curves peak between 15 and 20 kHz. This compares favourably with the theoretical peak of 15.3 kHz calculated from equation (23) using τ_D and τ_T values of 10.4 μs (Rodgers 1985) and 0.25 μs (Parker 1987). The solid curve fitted through the quadrature data was obtained by normalizing the imaginary $^{1}\text{O}_2$ component (equation (15)) to the experimental data (50 $\mu\text{g ml}^{-1}$) at 20 kHz. Optimum values of the in-phase component were then calculated by multiplication of equation (14) with the constant normalizing factor found from the quadrature data. As shown in Figure 4.4 the agreement between theory and experiment is quite good. The dashed horizontal line represents the relative in-phase output generated by the sensitizer infrared fluorescence. It was found by setting $[^{1}\text{O}_2]_R = 0$ (equation (14)), i.e., $\omega^2 \tau_T \tau_D = 1$. The in-phase signal at this ω is thus entirely due to fluorescence. The chopping frequency at which this occurred was approximately 99 kHz.

From the experimental results (50 $\mu\text{g ml}^{-1}$ PFII in MeOH), the 1272 nm quadrature signal ranged from a high of 151 μv (10 kHz) to a low of 7.2 μv (100 kHz) - well above the detector noise level (Figure 4.1). From 10-35 kHz, the 1201 nm in-phase (fluorescence only) component was slightly smaller than the 1272 nm quadrature component. Above and below this frequency range, the in-phase

component was found to be larger than the quadrature component at 1272 nm. At all frequencies tested, the 1201 nm in-phase component was observed to be larger than the 1303 nm in-phase component. This was expected since the 1201 nm filter has a slightly wider bandwidth (9.4 vs. 8.5 nm) and better peak transmission efficiency (54 vs. 44 %) than the 1303 nm filter. For example, at 2 kHz, the 1201 and 1303 nm in-phase components were 268 and 228 μv respectively. Had the 1303 nm filter had the same bandwidth and peak transmission efficiency as the 1201 nm filter, the 1303 nm in-phase component would have been approximately 274 μv . Thus differences in the in-phase components could be attributed entirely to differences in filter properties. This suggests that, over this spectral range, variations in the background fluorescence were negligible.

At all frequencies tested, the 1303 nm quadrature component did not return to the initially set zero found with the 1201 nm filter. The 1303 nm quadrature signal was approximately 13-15 % of the 1272 $^1\text{O}_2$ signal at all frequencies. This deviation from the initially set zero could not be attributed to phase drift or to "leaking" of the $^1\text{O}_2$ signal through the 1303 nm filter. As previously mentioned, phase drift was checked for and, in all but a few isolated cases, was not found to be a problem. Again, in those cases where phase drift was observed, the

experiment was repeated. As a double check, phase drift was checked for by zeroing the fluorescence signal emanating from a volunteer's irradiated fingertip and monitoring any changes in this zero as a function of time. In order to eliminate the possibility of phase drift due to temperature changes in the electronic components (0.1° per $^\circ\text{C}$), the lock-in was turned on 15 minutes prior to the experiment. The fact that the zero condition remained unchanged over the course of several minutes supports the earlier observations that phase drift was not a problem in any of the experiments performed in this work.

As evidenced from Figure 3.4, the large 1303 nm quadrature signal could not be attributed to overlap of the $^1\text{O}_2$ emission spectrum with the 1303 nm pass band. From Figure 3.4, it can be seen that the $^1\text{O}_2$ component is very close to zero at wavelengths greater than 1290 nm. The overlap of the $^1\text{O}_2$ emission with the 1303 nm filter can thus be considered negligible.

Having eliminated phase drift and overlap of the $^1\text{O}_2$ emission with the 1303 nm pass band, the larger than expected 1303 nm quadrature component was thought to be due to temporal and spectral differences between; (i) the fluorescence signals and/or (ii) the fluorescence and phosphorescence signals. Most photosensitizers, including PFII, have two fluorescence components which can be

distinguished based on their rate of decay. The fluorescence decay is a function of the aggregation state, hence the fast component is due to aggregated species while the slow component is due to monomers (Andreoni and Cubeddu 1984). Since PFII never exists in the pure monomeric or aggregated state, the two fluorescence components will be present in all environments. The relative intensities of the two components will however, vary with the environment. During the experiments, the sum of the fluorescence components was zeroed at 1201 nm. However, due to the different temporal and spectral behaviour of the fluorescence components, the sum was not necessarily zero at other wavelengths. The situation was complicated by the presence of the $^1\text{O}_2$ phosphorescence. Again, due to temporal and spectral differences, the fluorescence and phosphorescence signals were probably not zeroed at 1303 nm even though all three signals were zeroed at 1201 nm. The large 1303 nm quadrature signal is thus postulated to be due to temporal and spectral differences between the three luminescence signals. The contribution of triplet photosensitizer phosphorescence to the 1303 nm quadrature signal was uncertain since the photochemistry of PFII is poorly understood and the phosphorescence spectrum and yield is unknown. When the experiment was repeated using an aqueous solution of $50 \mu\text{g ml}^{-1}$ of PFII in PBS, the 1272

nm quadrature component was indistinguishable from noise at all frequencies examined. The inability to detect $^1\text{O}_2$ in this case was not surprising given the tendency of DHE to aggregate in aqueous solution (Kessel 1984). This aggregation was confirmed by observation of the characteristic blue-shift of the Soret band from 385 to 365 nm (Figure 4.8). A more thorough discussion of this effect is presented in a later section. Aggregation shortens the lifetime of the S_1 state (Andreoni et al. 1982) and results in very poor triplet yields (Dougherty 1987). In such a form then, it is neither very fluorescent in the visible portion of the spectrum nor a very efficient generator of $^1\text{O}_2$. In fact, transient absorption spectroscopy studies have shown negligible triplet formation (hence negligible $^1\text{O}_2$ formation) by PFII in aqueous solution (Redmond et al. 1982). Using literature values of $\tau_T = 2.4 \mu\text{s}$ (Parker 1987), $\tau_D = 3.2 \mu\text{s}$ (Parker 1987), $\mu_{1270} = 1 \text{ cm}^{-1}$ (Patterson et al. 1988) and measured values of $\mu_{\text{ap}} = 0.49 \text{ cm}^{-1}$ and $x = z = 0.5 \text{ cm}$, the estimated quantum yield (ϕ_{Δ}) of $^1\text{O}_2$ (using equation (22)) is less than 0.0030 for PFII in aqueous solution. This is six times smaller than the value found by Keir et al (1987) for DHE in aqueous solution (0.018).

The magnitude of the 1201 nm in-phase component was on average 10-20 % higher than the corresponding component

for PFII in MeOH ($50 \mu\text{g ml}^{-1}$). The reason for this is not fully understood since the behaviour of sensitizer infrared fluorescence as a function of aggregation state has not been studied. The observation does, however, suggest that aggregation does not inhibit fluorescence in the infrared to the same extent that it does in the visible portion of the spectrum. Aggregation is known to produce changes in the energy level structure of porphyrins. It appears that these changes cause a decrease in the transitions yielding photons in the visible while the transitions yielding infrared photons may remain largely unaffected.

4.2.3 Detection of $^1\text{O}_2$ in MeOH and PBS using ALSPc

The negative quadrature and in-phase components for ALSPc in MeOH and in PBS (both at concentrations of $2 \mu\text{g ml}^{-1}$) are shown in figures 4.5 and 4.6. As was the case with PFII, the quadrature component in MeOH peaks between 15 and 20 kHz. In order to fit the experimental data, knowledge of τ_T and τ_D was again required. Since the solvent used was MeOH, τ_D was again taken as $10.4 \mu\text{s}$. An extensive literature search failed to find a value for τ_T . The choice of a τ_T value in MeOH was not considered to be that critical since, in this environment, τ_D is expected to be much greater than τ_T . As a result, the location of the peak will be largely unaffected by the

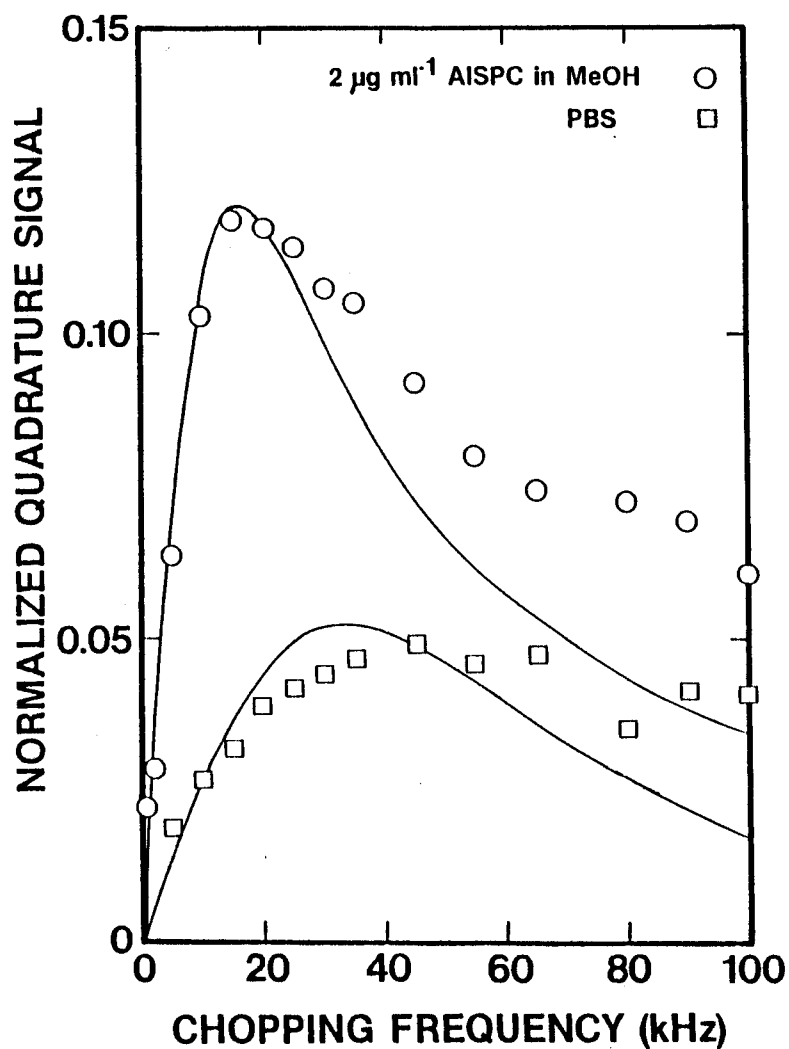


Figure 4.5 Normalized quadrature outputs versus chopping frequency for AlSPc in PBS and in MeOH.

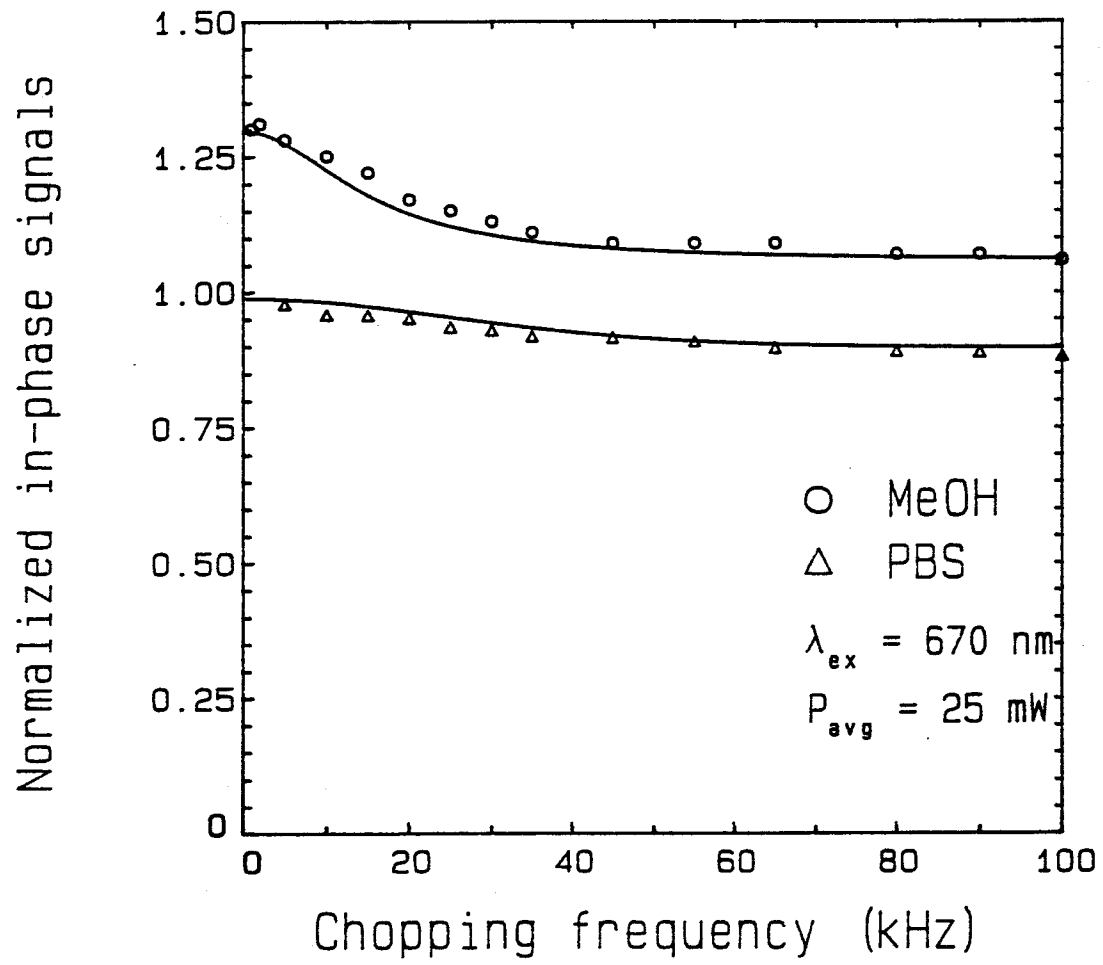


Figure 4.6 Normalized in-phase outputs versus chopping frequency for AlSPc in PBS and in MeOH ($2 \mu\text{g ml}^{-1}$).

choice of τ_T . For convenience a τ_T value of $0.25 \mu\text{s}$ was chosen. Using these τ_T and τ_D values, however, yielded poor quadrature and in-phase fits (normalized) as indicated in figures 4.5 and 4.6. To fit the PBS data, τ_D and τ_T values of 3.2 and $2.4 \mu\text{s}$ (Parker 1987) were used. Again, the normalized quadrature and in-phase fits were poor (figures 4.5 and 4.6). Fits were tried using various τ_D and τ_T combinations. However, they were no better than those obtained using the above lifetimes and matched to the experimental data at 15 (MeOH) and 45 kHz (PBS). The poor fits suggest that the simple first order kinetics described by Parker (1987) may not be applicable to AlSPc.

Examination of Figure 4.5 reveals that the magnitude of the relative PBS quadrature component is between 2-3 times lower than the corresponding MeOH component. Given that the in-phase 1201 nm components are approximately equal and that the $^1\text{O}_2$ quantum yields in aqueous solution (0.34 - Rosenthal et al 1986) and in MeOH (0.30 - Keir et al. 1987) are virtually identical, this reduction can be attributed to the fact that the $^1\text{O}_2$ lifetime in PBS ($3.2 \mu\text{s}$) is approximately three times shorter than the corresponding lifetime in MeOH ($10.4 \mu\text{s}$). According to equation (15), the quadrature component is proportional to τ_D . Thus, if τ_D decreases by a factor of

three, the quadrature component is also expected to decrease by approximately that same amount. This is in good agreement with the results in Figure 4.5. The lifetime difference in the two solvents is also responsible for the appearance of the peaks at different chopping frequencies. According to equation (23), the shorter τ_D , the greater the peak frequency. From equation (23), the peak in MeOH should occur at 15.3 kHz since the τ_D and τ_T values are identical to those used for PFII. This is in good agreement with the experimentally determined peak. In the PBS case, evaluation of equation (23) using τ_D and τ_T values of 3.2 and 2.4 μ s respectively, yields a peak frequency of 32.8 kHz. This is not inconsistent with the experimental results. From Figure 4.5, the PBS peak is very broad and is situated between 40 and 60 kHz. As can be seen, the peak region is very difficult to define since the quadrature component falls off very slowly with frequency.

In spite of the fact that the AlSPc solutions were diluted by a factor of 25 compared to the PFII solutions (2 vs. 50 μ g ml⁻¹), the absolute 1272 nm quadrature signals in MeOH were comparable. (Actually, the AlSPc values were 20-25 % lower than the corresponding PFII values.) Given that the ¹O₂ yields for the two photosensitizers are almost identical, this can be explained by the fact that the absorbance of AlSPc in MeOH at 670 nm is approximately

23 times greater than the absorbance of PFII in MeOH at 624 nm (figures 3.6a and b).

As previously mentioned, the 1201 nm in-phase components of AlSPc in MeOH and in PBS were virtually identical. This is not surprising since AlSPc exists in monomeric form in both solutions. However, the in-phase component of AlSPc in MeOH was approximately seven times larger than the corresponding PFII value in MeOH. This large fluorescent component is reflected in the rather flat normalized in-phase components (Figure 4.6). As previously mentioned, the normalized in-phase component is given by

$$\frac{\text{In-phase (1272 nm)}}{\text{In-phase (1201 nm)}} = \frac{\text{sens. IR fluor.} + {}^1\text{O}_2}{\text{sens. IR fluor.}}$$

Since the background fluorescence is very large and does not vary significantly over the narrow spectral range of interest, it is changes in the ${}^1\text{O}_2$ component which will dictate the shape of the normalized in-phase component. The quadrature " ${}^1\text{O}_2$ only" component in PBS was approximately three times lower than the corresponding component in MeOH. Since the 1201 and 1272 nm in-phase components were comparable, the background fluorescence was even more dominant, thus accounting for the flatter curve in Figure 4.6. As expected, due to the large background dominance, the normalized in-phase PBS data points were closer to

unity than the corresponding MeOH data.

An examination of figures 4.4 and 4.5 reveals that the normalized quadrature component of AlSPc in MeOH is 7-10 times smaller than the corresponding PFII component. Again, this can be attributed to the much larger background fluorescence of AlSPc in MeOH. If the in-phase component is approximately seven times larger than the corresponding PFII component, and if the quadrature components of the two photosensitizers are comparable, then it follows that the ratio of the quadrature " $^{1}O_2$ only" component to the in-phase "fluorescence only" component will be approximately seven times smaller in the AlSPc case.

As was the case with PFII, the 1303 nm in-phase component was observed to be smaller (by ca. 10 %) than the corresponding 1201 nm component. Again, this discrepancy was attributed to differences in the properties of the two filters. A similar pattern was observed for AlSPc in PBS. However, in this case, the 1303 nm signal was approximately 25 % smaller than the in-phase signal at 1201 nm. This larger difference might have been due to a small wavelength dependence of the infrared fluorescence.

As was found with PFII, the 1303 nm quadrature component did not return to the initially set zero found with the 1201 nm filter. As for PFII, in both MeOH and PBS, the 1303 nm quadrature signal was approximately 10-15 % of

the 1272 nm quadrature signal. Possible explanations for this discrepancy were described in the previous section.

4.3 Detection of $^1\text{O}_2$ in vivo

4.3.1 Introduction

Having shown that the system was capable of $^1\text{O}_2$ detection, the main objective of this series of experiments was to determine whether the system was capable of detecting $^1\text{O}_2$ in a complex heterogeneous biological environment. As well, it was hoped that information could be obtained regarding the $^1\text{O}_2$ lifetime and hence determine the specific type of environment (i.e., aqueous, lipid, protein) in which this cytotoxic agent was generated. This is an important question since the choice of chopping frequency for maximum $^1\text{O}_2$ signal is strongly dependent on the environment, i.e., the $^1\text{O}_2$ lifetime.

4.3.2 $^1\text{O}_2$ detection in mice injected with PFII

The results for the PFII injected mice are summarized in figures 4.7a and 4.7b. On inspection, a pattern emerges for the normalized 1272 nm quadrature components in Figure 4.7a. That is, for the two injected groups of mice studied, there seems to be an increase in signal with chopping frequency. However, there do not appear to be any well defined peaks. These observations are in contrast with those of Parker (1987) who reported peaks

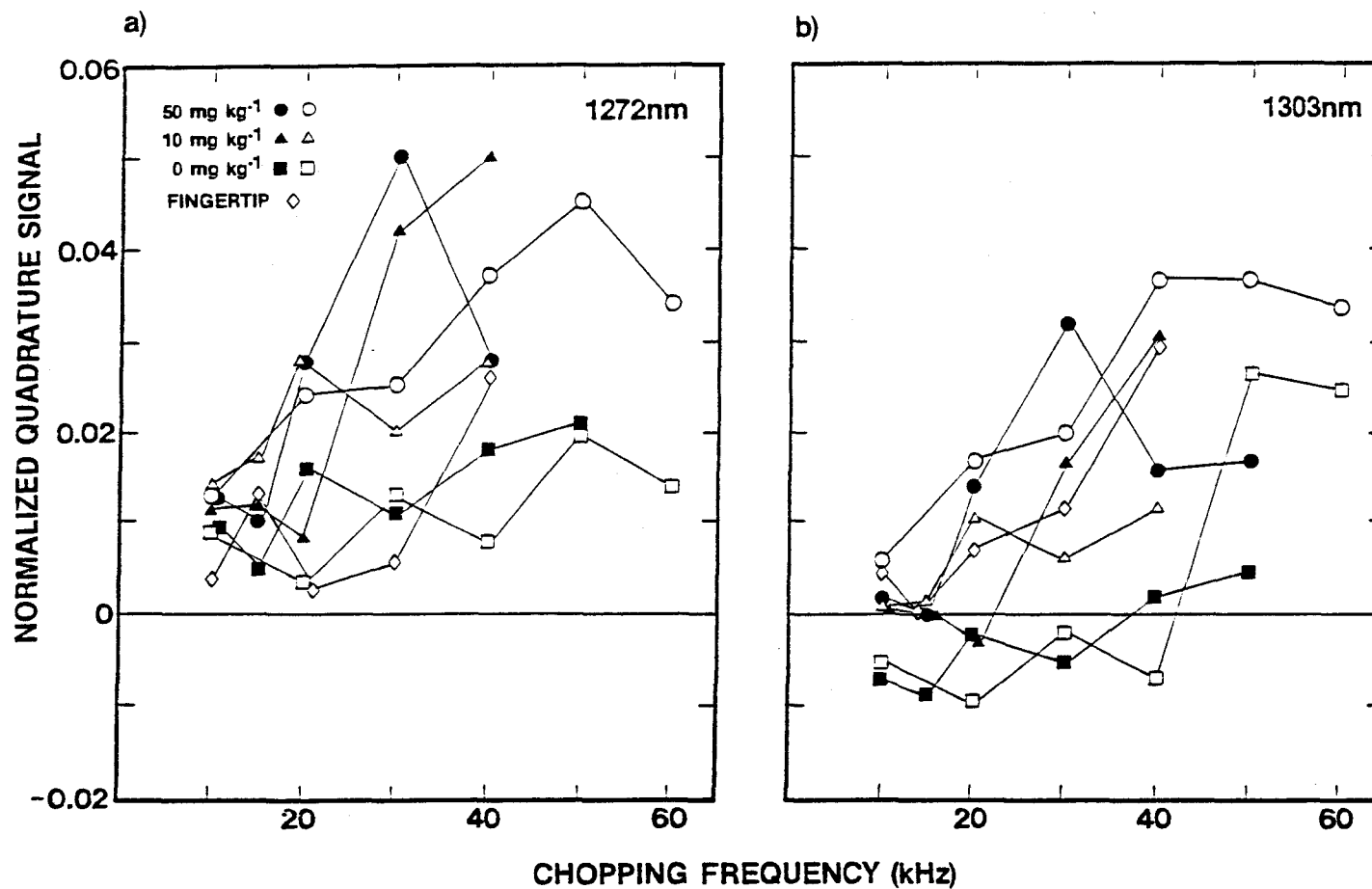


Figure 4.7a 1272 nm quadrature outputs in vivo versus chopping frequency.
 Figure 4.7b 1303 nm quadrature outputs in vivo versus chopping frequency.

located at approximately 14 kHz. From Figure 4.7a it can be seen that, for mice injected with the same level of PFII, the results were not in close agreement. This was not surprising since a certain amount of variability can be expected in biological experiments of this sort.

Furthermore, it should be noted that the signals observed from the injected mice were not significantly larger than those observed from the controls.

Examination of Figure 4.7b reveals that the normalized 1303 nm quadrature signal followed the same pattern as the corresponding 1272 nm signal and the magnitude of the two signals were roughly equivalent. This emission is thus not characteristic of 1O_2 .

As expected (Parker 1987), due to tissue autofluorescence, the 1201 nm in-phase component was on average an order of magnitude larger than the corresponding fluorescence component obtained for PFII in MeOH ($50 \mu\text{g ml}^{-1}$). No significant differences in fluorescence were observed between injected and control mice and the signal obtained from the fingertip of a volunteer was also comparable. This suggests that most of the observed fluorescence was due to normal tissue components and not PFII.

Although this series of experiments failed to detect 1O_2 , a marked response was observed for the

irradiated mice four days post treatment. Compared to the controls, in which no gross damage was observed, the mice injected with 10 mg kg^{-1} PFII exhibited noticeable skin damage. In one case, the tumour, which had become greatly enlarged, showed evidence of necrosis in the immediate area of irradiation. In both cases the skin was burned and had become very leathery, but not to the same extent as the 50 mg kg^{-1} group. The mice in the 50 mg kg^{-1} group both exhibited strong evidence of tumour necrosis. Their skin had blackened and become very tough. In one case, the interior lateral toe had fallen off. From the evidence presented above, it is clear that the injected mice responded to treatment. However, it is not clear whether the damage was caused by $^1\text{O}_2$ or some other radical such as superoxide. This problem is unlikely to be resolved based on the results of this series of experiments, however, examination of some of the anomalous results, such as the large 1303 nm quadrature signal, may provide some clues. As previously discussed, the origin of the large 1303 nm quadrature signal might be due to differences in the temporal and spectral behaviour of the fluorescence and phosphorescence signals. It is possible that the large 1303 nm signal might have been caused by phosphorescence and/or fluorescence from radicals such as superoxide. Another possibility involves transmission of a significant

component of the $^1\text{O}_2$ emission through the 1303 nm bandpass filter. This was seriously considered since the $^1\text{O}_2$ emission spectrum is a function of the environment. According to Parker (1987), the biological environment induces quite a noticeable shift in the central emission wavelength - from 1270 nm to approximately 1260 nm. However, since the shift is away from 1300 nm, the large signal could not be attributed to environmentally induced changes in the $^1\text{O}_2$ emission spectrum. It is possible, however, that the 1272 nm filter might be missing some of the $^1\text{O}_2$ signal due to this peak shift. Although this possibility cannot be discounted, the reduction in signal is unlikely to be significant due to the large bandpass of the 1272 nm filter (18 nm FWHM). A thorough investigation of this interesting problem could not be undertaken due to a lack of bandpass filters around 1260 nm. Finally, the similarity between the quadrature signals at 1303 and 1272 nm might be due to quenching of $^1\text{O}_2$ by biomolecules in vivo. As will be discussed later, quenching lowers the lifetime of $^1\text{O}_2$ thus producing a decrease in the absolute magnitude of the 1272 nm quadrature signal.

In summary then, the similarity in quadrature signals obtained with the 1272 and 1303 nm filters might be due to; (i) a reduction in the 1272 nm quadrature signal as a result of an environmentally induced shift in the central

emission wavelength of $^1\text{O}_2$, (ii) a reduction in the 1272 nm quadrature signal due to quenching by biomolecules, (iii) luminescence phenomena arising from processes other than those involving $^1\text{O}_2$.

4.4 Detection of $^1\text{O}_2$ in protein-aqueous solution

4.4.1 Introduction

The in vivo experiments failed to detect $^1\text{O}_2$ luminescence. Since in-vivo photochemistry may be very complicated, it was decided to attempt measurements in a more controllable homogeneous environment. A protein environment was chosen since PFII is known to bind non covalently to plasma serum proteins such as human serum albumin (Rosenthal et al 1986).

4.4.2 Detection of $^1\text{O}_2$ in a 10 % solution of FCS and PBS using PFII ($50 \mu\text{g ml}^{-1}$)

At all frequencies tested the 1272 nm quadrature component was equal to the noise level, i.e., no $^1\text{O}_2$ signal was detected. The absolute magnitude of the 1201 nm in-phase signal was identical to that observed for PFII in PBS.

The inability to detect $^1\text{O}_2$ in this case was thought to be due to either quenching or aggregation. There seems to be some confusion concerning the binding of PFII to serum proteins. Redmond et al (1985) have found that

PFII binds to these proteins in aggregated form while Grossweiner's (1985) observations suggest disaggregation of PFII upon binding to serum proteins. If disaggregation occurs upon PFII binding, the lack of an observable 1O_2 signal is probably due to protein quenching. If, on the other hand, PFII binds to serum proteins in aggregated form, then the lack of a signal is probably due to the fact that the sensitizer is a very poor 1O_2 generator in such a form.

To test whether the lack of a signal was due to aggregation, Soret band absorption spectra of three different PFII solutions (MeOH, PBS and 10% FCS and PBS) were examined (Figure 4.8). Porphyrins exhibit very strong absorption in this band which is approximately 50 nm wide and is located between 300 and 400 nm. The exact location of the Soret peak is a function of the degree of porphyrin aggregation. Disaggregation of porphyrins results in a red shift of the Soret peak (Poletti et al. 1984). PFII is known to exist in a monomeric state in MeOH and in an aggregated state in PBS. Now, if PFII exists in an aggregated state in 10 % FCS and PBS, its absorption peak should be located at approximately the same wavelength as the solution of PFII in PBS. Conversely, if PFII exists in a monomeric state in 10 % FCS and PBS, its absorption peak should be located in the vicinity of the PFII in MeOH peak.

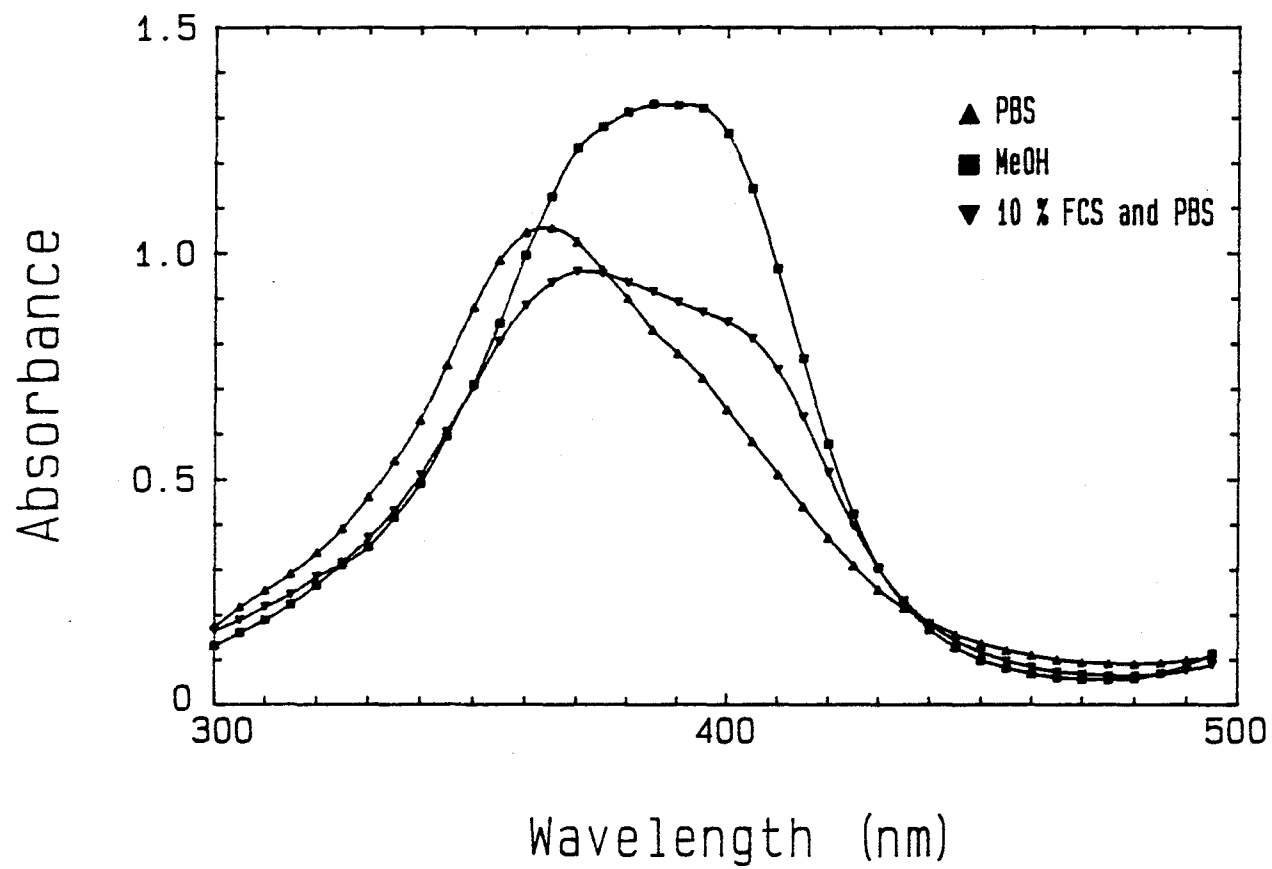


Figure 4.8 Soret band absorption spectra of PFII in various solutions ($5 \mu\text{g ml}^{-1}$).

From Figure 4.8, the 10 % FCS and PBS absorption curve appeared to be a weighted sum of the two other curves with two roughly equal peaks at 370 and 395 nm indicating the presence of a disaggregated fraction. In spite of such a fraction, no $^1\text{O}_2$ signal was observed. The lack of a signal was thus thought to be due to protein quenching. In order to investigate this further, the experiment was repeated using AlSPc.

4.4.3 Detection of $^1\text{O}_2$ in a 10 % solution of FCS and PBS using AlSPc ($2 \mu\text{g ml}^{-1}$)

The 1201 nm in-phase component was approximately 1.5 times smaller than that observed with AlSPc in PBS. Similarly, the 1272 nm quadrature component was between 1.5 and 2.0 times smaller than that observed in the PBS experiment. Since AlSPc remains monomeric in aqueous solution (Darwent et al. 1982), the small $^1\text{O}_2$ signal cannot be attributed to aggregation. It was thought that since AlSPc, like PFII, binds non covalently to serum proteins (Rosenthal et al. 1986), the reduction in signal was most likely due to protein quenching. Evidence for protein quenching is shown in Figure 4.9 where the normalized quadrature component has been plotted. No attempt was made to fit the data since τ_D and τ_T were unknown for this environment. Normalized quadrature components from the other AlSPc experiments have been plotted for comparative

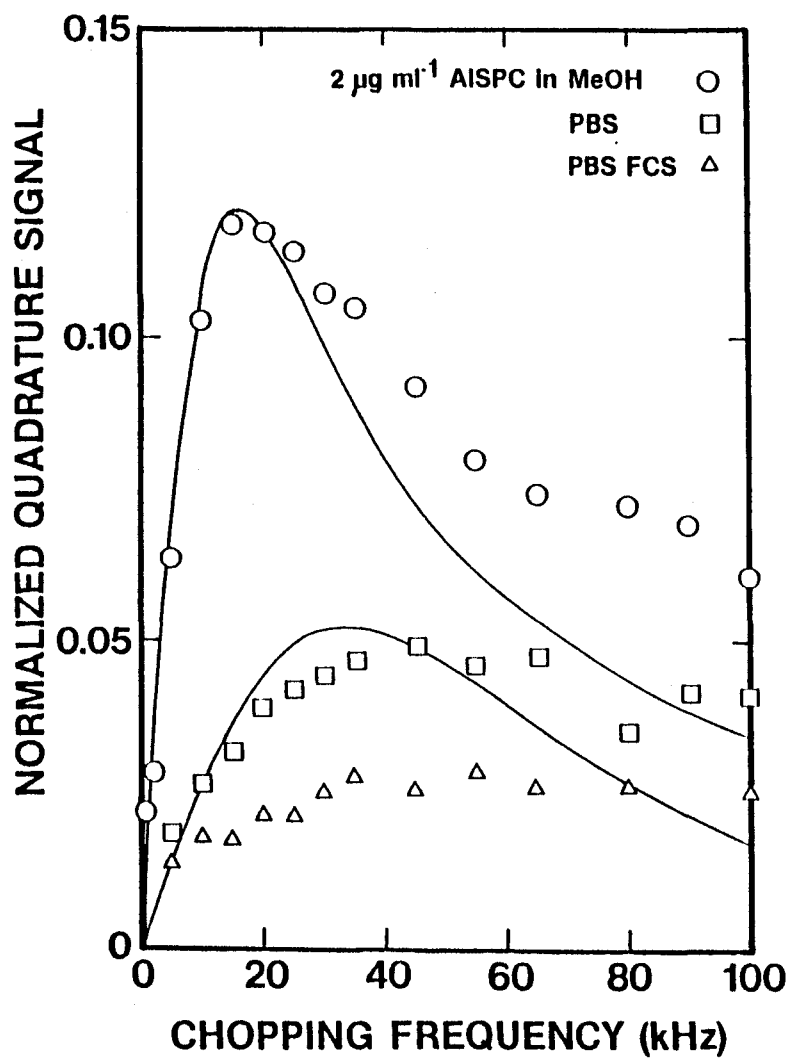


Figure 4.9 Normalized quadrature outputs versus chopping frequency for AISPC in various solutions.

purposes. The normalized quadrature component in this case is quite noisy and the peak is poorly defined. However, compared to the PBS data, it appears that the peak has been shifted to a slightly higher frequency. From Figure 4.9, the magnitude of the normalized quadrature component is approximately 1.5 times smaller than the corresponding PBS component. This suggests that τ_D (FCS and PBS) $\approx 2/3 \tau_D$ (PBS). If $\tau_D \approx \tau_T$ then, according to equation (23), the peak should be located at 43.8 kHz. This is not inconsistent with the experimental results. It thus appears that τ_D has been reduced by a small amount. This reduction is probably due to protein quenching. It should be emphasized however, that the broadness of the quadrature peak in Figure 4.9 really does not permit an accurate determination of τ_D in this protein environment. A more detailed experiment with varied protein concentration would probably clarify this.

4.5 Detection of 1O_2 in cell suspensions

4.5.1 Introduction

Detection of 1O_2 in even a relatively simple medium, such as FCS in PBS was shown to be non trivial. No 1O_2 was observed in the PFII case and only a weak signal was observed when using AlSPc. Certainly, the data obtained did not permit a determination of the 1O_2 lifetime in this

seemingly simple protein environment.

The cell culture experiments represented a final attempt at detecting $^1\text{O}_2$ in biological media. As well, it was hoped that an estimate of ζ_D in such media could be found. The advantage of working with cell cultures is that various parameters, such as suspension medium and cell concentration, can easily be varied. For example, the suspension medium can be chosen to reflect an aqueous or a protein-rich environment. On the other hand, maximum cell concentrations are limited and oxygen depletion is also a potential problem.

4.5.2 Detection of $^1\text{O}_2$ in cell suspensions using PFII and AlSPc

In total, ten cell culture experiments were performed. PFII was used in three of the experiments while AlSPc was used in five. The remaining two experiments were controls with no photosensitizer. Initial conditions and a summary of the results are presented in Table 4.1.

The number of viable cells ml^{-1} (column 5) was determined just prior to irradiation and the cell viability (column 9), evaluated following irradiation, is given by

$$\frac{\text{No. of live cells}}{\text{No. of (live + dead cells)}} \times 100 \%$$

The total light fluence values listed in column 8 were

Table 4.1 Summary of cell suspension results

Photosensitizer	Incubation Time (hr)	Wash and Spun	Suspension Medium	[cell] (viable cells/ml)	Irradiation Time (min)	Avg. Power (mW)	Total Fluence ($J\ cm^{-2}$)	Cell Viability (%)
PFII	18	no	Medium 1	1.42×10^6	30	26	234	0
PFII	18	yes	PBS	1.42×10^6	40	25	300	0
control	18	yes	PBS	2.70×10^6	30	25	225	100
PFII	48	yes	PBS	1.10×10^7	40	26	312	0
control	48	yes	PBS	2.70×10^7	40	26	312	90
AlSPc	18	yes	Medium 2	4.74×10^5	35	19	200	90
AlSPc	18	yes	PBS	1.40×10^5	30	19	171	60
AlSPc	18	yes	Medium 2	2.84×10^6	25	19	143	95
AlSPc	18	yes	PBS	1.74×10^6	30	19	171	54
AlSPc	43	yes	Medium 2	2.12×10^7	30	21	189	66

Medium 1 = Opti-MEM I and 10 % FCS.

Medium 2 = Opti-MEM I and 5 % FCS.

evaluated based on a beam area of 0.2 cm^2 . Each fluence was that incident at the cuvette, but the mean fluence "seen" by any one cell could be considerably less than this due to self absorption and fluid motion in the cuvette.

The initial PFII trials were performed at a concentration of approximately 10^6 viable cells ml^{-1} . No $^1\text{O}_2$ signal was observed. The 1201 nm "fluorescence only" component observed in the first trial was about 1.5-2.0 times larger than that observed in the second trial. This was attributed to the presence of photosensitizer in the medium since, in the first trial, the cells had not been washed. In the absence of photosensitizer (controls), the "fluorescence only" component was approximately an order of magnitude lower. The small amount of fluorescence observed in the controls was attributed to cell fluorescence. The 1201 nm "fluorescence only" component observed in the second trial was approximately three times lower than that observed for PFII in PBS, and approximately 15-25 times lower than was observed for the PFII injected mice. The large difference between cell and in vivo fluorescence was due mainly to the low concentration of cells used in the in vitro experiments. In spite of the fact that no $^1\text{O}_2$ was observed, the cells did respond to the treatment as evidenced by the 0 % cell viability. It was decided to repeat the

experiments using a higher cell concentration - approximately 10^7 viable cells ml^{-1} . However, as before, no signal was observed. Again, the 0 % viability indicated that the cells responded to treatment. The 1201 nm "fluorescence only" component was approximately 1.5 times larger than was observed in the second trial. This was due to the greater cell density used in this trial. It is interesting to note that the cell viability of the high density control group was around 10 % lower than that of the low density control group. This was attributed to the fact that cells do not fare as well in crowded environments. In general, the greater the cell concentration, the lower the cell viability.

The experiments were repeated using AlSPc in place of PFII. The first two experiments were performed at a low cell concentration - approximately 10^5 viable cells ml^{-1} . As was the case with PFII, no 102 was observed. As expected, due to equal cell densities, the "fluorescence only" components were comparable in the two cases. However, there was a significant difference in cell viability (30 %) between the cells suspended in medium and 5% FCS and those suspended in PBS. As shown in Table 4.1, this pattern was repeated throughout the AlSPc trials. This dependence of cell viability on the suspension medium is due to the fact that PBS is a "hostile" cell environment since it does not

contain any of the nutrients necessary for cell survival. As seen in Table 4.1, the cell responses in the two different media (90 and 60 % viabilities) were far from that obtained using PFII (0 % viability).

The experiments were repeated at a higher cell concentration - ca. 10^6 viable cells ml^{-1} . Again, no $^{10}\text{O}_2$ was observed. However, it should be noted that, due to an unfortunate mistake, the cell cultures used in these two trials were irradiated at 624 nm instead of the usual 670 nm. This prevented a comparison of the "fluorescence only" components with the lower concentration samples. As expected, the in-phase components were nearly identical for the two samples. In spite of the fact that the treatment was carried out at the wrong wavelength, the cell viabilities (95 and 54 %) were in good agreement with those obtained in the previous two trials indicating a response to the procedure. This is somewhat surprising since the absorption coefficient at 670 nm is approximately 10 times higher than at 624 nm.

A final attempt at $^{10}\text{O}_2$ detection was made using a very high cell concentration - approximately 10^7 viable cells ml^{-1} . A small 1272 nm quadrature signal was observed. Unfortunately, as for the mouse experiments, the 1303 nm quadrature signal was of the same magnitude. As a result, it cannot be concluded that $^{10}\text{O}_2$ was responsible for the

cell damage as reflected in the 71 % viability. The "fluorescence only" component was very high - approximately 15-20 times higher than the low concentration (10^5 viable cells ml^{-1}) case. Again this was attributed to a much greater cell density.

Finally, from Table 4.1 it can be seen that cell viability depends very strongly on the type of photosensitizer used. Cell viabilities when using PFII were much lower than the corresponding AlSPc values. It thus appears that PFII is more phototoxic than AlSPc. This is contrary to the findings of van Lier et al. (1988) and Chan et al. (1986) who both found that AlSPc was approximately twice as phototoxic as PFII on a dose basis. It was thought that the origin of this discrepancy might be due to the fact that different cell lines respond differently to the two photosensitizers. As well, uptake may vary with the cell line. It is known that AlSPc is less cytotoxic to cells, maintained in darkness or exposed to room light, compared to PFII (Chan et al. 1986). This agreed well with the observation that, on average, only 50 % of the PFII cells survived incubation, while approximately 80 % of the AlSPc cells survived this procedure. This observation however, cannot explain the difference in phototoxicity since, as previously mentioned, cell death due to the incubation procedure was accounted for in determining the

cell viability. The reason for the difference in phototoxicity remains unexplained.

At any rate, regardless of the photosensitizer used, the fact remains that, like the *in vivo* experiments, no $^1\text{O}_2$ was observed during PDT of cell suspensions in spite of the fact that extensive cell death was documented. There are two possible explanations for the lack of a signal *in vivo* and *in vitro* (using the cell suspensions):

- (1) $^1\text{O}_2$ is not produced in biological environments and the toxic effects are due to other processes.
- (2) $^1\text{O}_2$ is rapidly quenched by biomolecules thus reducing its lifetime to the point where it cannot be detected.

Given the ample evidence to support the generation of $^1\text{O}_2$ *in vivo* (Weishaupt et al. 1976 and Moan et al. 1979), the second scenario appears much more plausible. According to Rodgers (1988), the $^1\text{O}_2$ lifetime in biological media can be expressed as

$$D = \{k_r + k_{nr} + \sum_i k_{qi} [Q_i]\}^{-1} \quad (26)$$

where k_r and k_{nr} are the radiative and non-radiative (solvent induced) decay rate constants respectively. The terms inside the summation refer to the rates of quenching (or chemical reaction) induced by other molecules (Q_i) present in the environment.

In steady state measurements, such as the ones performed in this work, the signal amplitude is directly proportional to τ_D (equation (15)). Thus, if the quenching term in equation (26) is significant, as is the case in biological media, the signal amplitude will be reduced to such an extent that detection is no longer possible even with the sensitive system used in this work. Furthermore, a reduction in τ_D results in a shift in the peak chopping frequency towards higher frequencies (equation (23)). This is rather unfortunate since, according to Figure 4.2, the NEP increases at higher frequencies. However, if $\tau_D \ll \tau_T$, the peak will be located at $(\tau_T)^{-1}$ according to equation (23). Thus, at very low 1O_2 lifetimes, the lack of a signal is almost entirely due to a reduction in signal amplitude rather than to a shift in the peak chopping frequency since the location of the peak will be determined by the triplet lifetime.

If the lack of a 1O_2 signal in vivo is due to quenching, then the results of this work allow an estimation of the lower limit for the lifetime of 1O_2 in this environment. Such a calculation is shown in the following section.

4.6 Estimation of the 1O_2 lifetime in vivo

The calculations were performed for the case of the mouse footpad tumours using the 50 mg kg⁻¹ PFII injected group. Equation (21) was solved for τ_D using the sensitivity values found in Figure 4.1 and using a ϕ_{Δ} value of 0.25. The incident fluence rate, ψ_0 , was directly measured and, as previously discussed, $\mu_{ex} = \mu_{1270} = 5 \text{ cm}^{-1}$. The tissue thickness (t) was taken to be 1 cm and, the photosensitizer concentration in the tumour was estimated at 50 $\mu\text{g ml}^{-1}$ at 24 hr post injection (Wilson et al. 1988). The value of μ_{ap} was thus taken to be 0.93 cm^{-1} . The triplet lifetime (τ_T) was not known since the chemical environment in vivo is uncertain. A value of 9.6 μs was used by Parker (1987) corresponding to an aqueous environment with physiological oxygenation. This is clearly an upper bound value, thus τ_D values have also been calculated for $\tau_T = 0.25$ and 3.2 μs .

As previously mentioned, the signals obtained in vivo showed a wavelength dependence uncharacteristic of that expected from 1O_2 . A significant luminescence background (fluorescence, phosphorescence or a combination of both) was observed. However, if this luminescence background is ignored, the lower limit on the 1O_2 lifetime can be approximated by the detector rms noise.

Equation (21) was thus solved for a given value of ω by setting $S_q(\omega)$ equal to the rms noise at that frequency. Table 4.2 shows that the lifetime of 1O_2 is unlikely to be lower than 0.1 μ s. in tissue. In Table 4.2 the measurement point that fixes the lowest limit is shown in bold face.

The short 1O_2 lifetime would explain the failure of other investigators (Rodgers 1988) to observe 1O_2 and would also be in agreement with Matheson et al. (1975) who report 1O_2 lifetimes of less than 1 μ s in physiological protein concentrations. If this quenching is due to amino acids, as postulated by Matheson et al. (1975), the 1O_2 is not produced in a lipid environment such as the cell membrane. This is in agreement with Firey and Rodgers (1988) who postulated that, in erythrocyte cell ghosts, the lack of a 1O_2 signal is due to binding of the photosensitizer to intracellular components such as proteins. In this environment, the 1O_2 molecules will diffuse only a very short distance before being quenched by various intracellular components. Evidently then, due to rapid quenching, it appears that very few 1O_2 molecules survive for long in the intracellular environment, thus accounting for the lack of a signal in the mice and cell suspension experiments.

These observations do not agree with those of Parker (1987) who reported the detection of 1O_2 in vivo

Table 4.2 Calculations of the $^1\text{O}_2$ lifetime (lower limit) in vivo.

Chopping Frequency (kHz)	Triplet Lifetime (μs)		
	9.60	2.50	0.25
	$^1\text{O}_2$ Lifetime (μs)		
1	1.04	2.89	3.19
2	0.39	1.07	1.84
5	0.12	0.38	0.92
10	0.063	0.17	0.56
15	0.062	0.13	0.46
20	0.068	0.11	0.41
25	0.075	0.099	0.36
30	0.087	0.093	0.34
35	0.098	0.087	0.31
45	0.13	0.084	0.28
55	0.15	0.083	0.25
65	0.18	0.084	0.23
80	0.23	0.090	0.20
90	0.27	0.099	0.20
100	0.30	0.10	0.18

under conditions very similar to those described in this work but for a different tumour model. Parker's evidence of a quadrature signal at 1270 nm is inconclusive since such a signal was also observed in this work, however it was found to have the wrong wavelength dependence. Parker does show a measured spectrum of the quadrature signal peaking around 1260 nm, however, the spectrum is very noisy and results were not presented for a number of animals including controls. On close examination then, Parker's results are very much like those observed in this work, however, the conclusions reached are different.

4.7 Future developments

The results of this work suggest that, while in vivo monitoring of $^1\text{O}_2$ would be extremely useful in the development of PDT, it is improbable that infrared luminescence will provide such a tool. A more thorough understanding of the sensitizer photochemistry is required in order to quantitatively explain some of the anomalous results obtained in this work. This is especially true in the case of AlSPc, where the results of the simple solution experiments did not agree with theory suggesting a deviation from the simple kinetics proposed by Parker (1987). Perhaps in future experiments, it would be a good

idea to use photosensitizers whose photochemistry is more thoroughly understood, even though these are not used clinically. Furthermore, it would be useful to measure the detailed spectrum of the in-phase and quadrature emission for the in vivo case in order to clarify the findings.

The detector used was ideally suited for the measurements performed in this work since, in most cases, the location of the minimum NEP (ca.10 kHz) matched that of the $^1\text{O}_2$ peak (15-20 kHz). However, improvements in the system sensitivity could be accomplished by using higher laser powers and more sophisticated collection optics. Such improvements would greatly be aided by the development of more reliable laser sources. It is important to realize, however, that clinical doses of photosensitizers are an order of magnitude lower than the doses used in these experiments and that the ultimate goal is not only the detection of the $^1\text{O}_2$ signal but its measurement. Due to the limits on laser power imposed by hyperthermia, a useful clinical system would in all likelihood require a sensitivity of at least one or two orders of magnitude greater than the one developed in this work. Since the detector used in these experiments was state of the art, further improvements in the detection of $^1\text{O}_2$ must await the development of better detectors. Such developments are unlikely in the near future.

CHAPTER 5

CONCLUSIONS

A non-invasive system was set up to detect the near-infrared emission resulting from the de-excitation of $^1\text{O}_2$ during PDT. Evidence for the correct functioning of the system included; (i) the good agreement between calculated and quoted NEPs, and (ii) the close fit of the theoretical curves to the experimentally determined data using PFII in MeOH. As expected, due to PFII aggregation, no $^1\text{O}_2$ signal was observed in aqueous environments. The estimated $^1\text{O}_2$ quantum yield in PBS (< 0.0038) was somewhat different than that found by other investigators. $^1\text{O}_2$ signals were obtained in both organic and aqueous environments when using AlSPc. This was not surprising since AlSPc is known to remain monomeric in both environments. The poor fit of the theoretical curves to the experimental data, however, suggested a deviation from the simple kinetics presented in this work.

The fluorescence observed in vivo was approximately an order of magnitude greater than that observed in the PFII-MeOH solution ($50 \mu\text{g ml}^{-1}$). Most of this fluorescence was attributed to normal tissue components rather than to

PFII. The most significant in vivo observation was that the 1272 and 1303 nm quadrature signals were nearly identical suggesting that the emission was not characteristic of $^1\text{O}_2$. In spite of the fact that $^1\text{O}_2$ luminescence was not observed, there was a marked response among the mice to the treatment. A similar pattern was observed in the cell culture experiments. In all but one of the eight experiments involving either AlSPc or PFII, no quadrature signal was observed at 1272 nm. In the one instance where such a signal was observed, the 1303 nm quadrature signal was found to be equivalent. Thus it could not be concluded that the extensive cell death observed was due to $^1\text{O}_2$.

The lack of a $^1\text{O}_2$ signal in the mouse and cell culture experiments was thought to be due to rapid quenching of $^1\text{O}_2$ by biomolecules. Such quenching was thought to reduce the $^1\text{O}_2$ lifetime to such an extent that it could no longer be detected, even with the sensitive system used in this work. This quenching phenomenon was consistent with the results of the experiments involving protein-aqueous solutions.

Since $^1\text{O}_2$ was not observed in mice or in cell cultures, its lifetime in biological environments could not be determined directly. However, the results of this work allowed a lower limit to be estimated for the $^1\text{O}_2$ lifetime in vivo - approximately 0.1 μs . This is in good agreement

with other investigators and suggests that 1O_2 is produced and quenched in a protein rather than in a lipid environment. It is therefore unlikely that 1O_2 is generated in the cell membrane.

The short 1O_2 lifetime in biological environments explains the lack of an observable signal in the mouse and cell culture experiments. Since the best available detector was used in this work and, since a useful clinical system would probably require a sensitivity of 1-2 orders of magnitude greater than this, it appears unlikely that remote monitoring of the infrared 1O_2 phosphorescence during PDT will be possible in the near future. Such a development will have to await the discovery of more sensitive detectors.

APPENDIX A

DERIVATION OF DETECTOR RESPONSE

The measured impulse response of the detector to a background event is shown in Figure A1. Since the signal decays exponentially (Figure A2) to 37 % of its original value in 30.8 μ s, the impulse response can be given by

$$I(t) = (\tau^{-1}) e^{-t/\tau} H(t) \quad (1A)$$

where $\tau = 30.8 \mu$ s is the time constant and $H(t)$ is the Heavyside function. According to Bracewell (1978):

$$\text{F.T.}[e^{-x}H(x)] = \frac{1 - i2\pi f}{1 + (2\pi f)^2} \quad (2A)$$

Using the similarity theorem and f as the frequency variable:

$$\text{F.T.}(\tau^{-1}) [e^{-t/\tau} H(t)] = \frac{1 - i2\pi \tau f}{1 + (2\pi \tau f)^2} \quad (3A)$$

When measuring the frequency response, $R(f)$, one is just looking at the amplitude of the F.T. in equation (3A). The frequency response is thus given by:

$$R(f) = \left[\left(\frac{1 - i2\pi \tau f}{1 + (2\pi \tau f)^2} \right) \left(\frac{1 + i2\pi \tau f}{1 + (2\pi \tau f)^2} \right) \right]^{1/2} \quad (4A)$$

Upon simplification:

$$R(f) = [1 + (2\pi \tau f)^2]^{-1/2} \quad (5A)$$

Normalization of $R(f)$ to $B(\omega)$ at 2 kHz yields the theoretical curve in Figure 4.1. From equation (5A), it can be shown that for large f , $R(f) \propto f^{-1}$, i.e., a log-log plot of $R(f)$ vs f should yield a slope of -1 . This is in excellent agreement with the slope found at frequencies above 10 kHz (Figure 4.1).

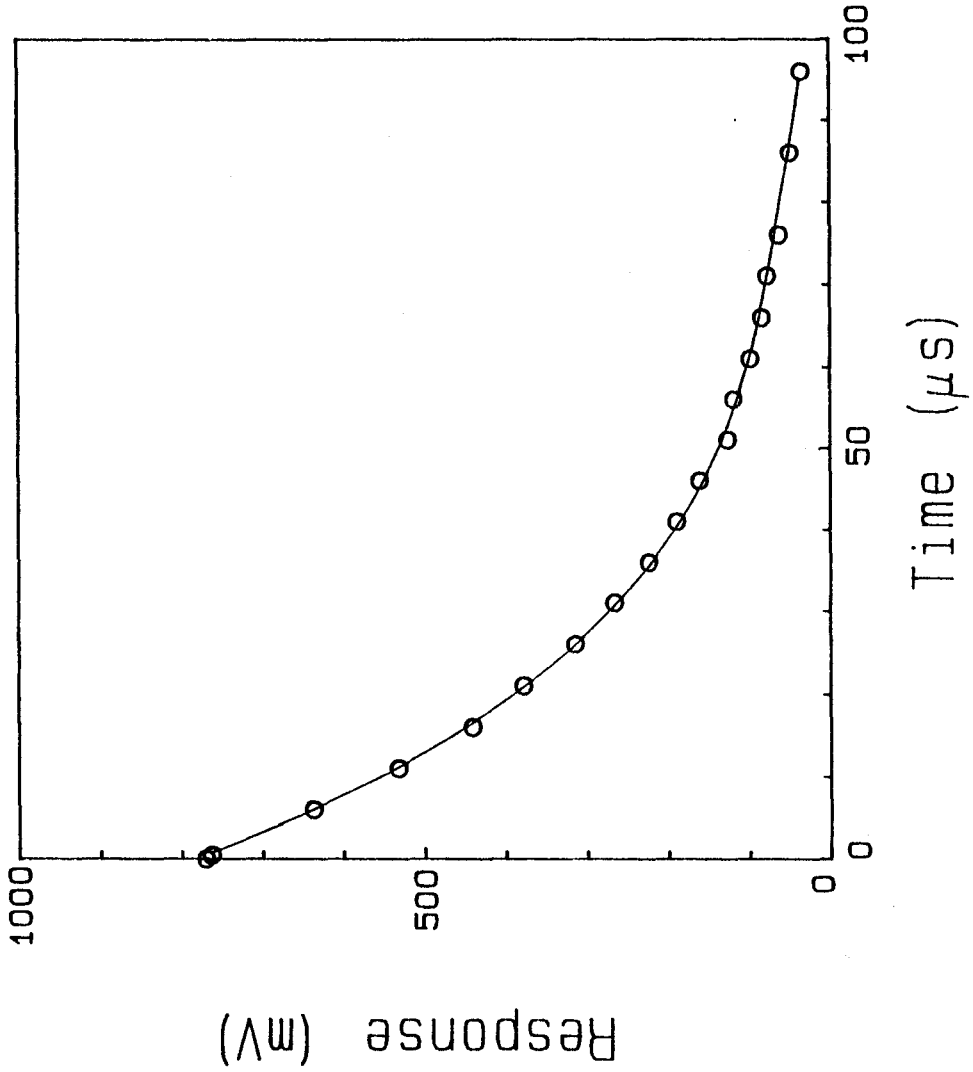


Figure A1 Impulse response of the E0-817S.

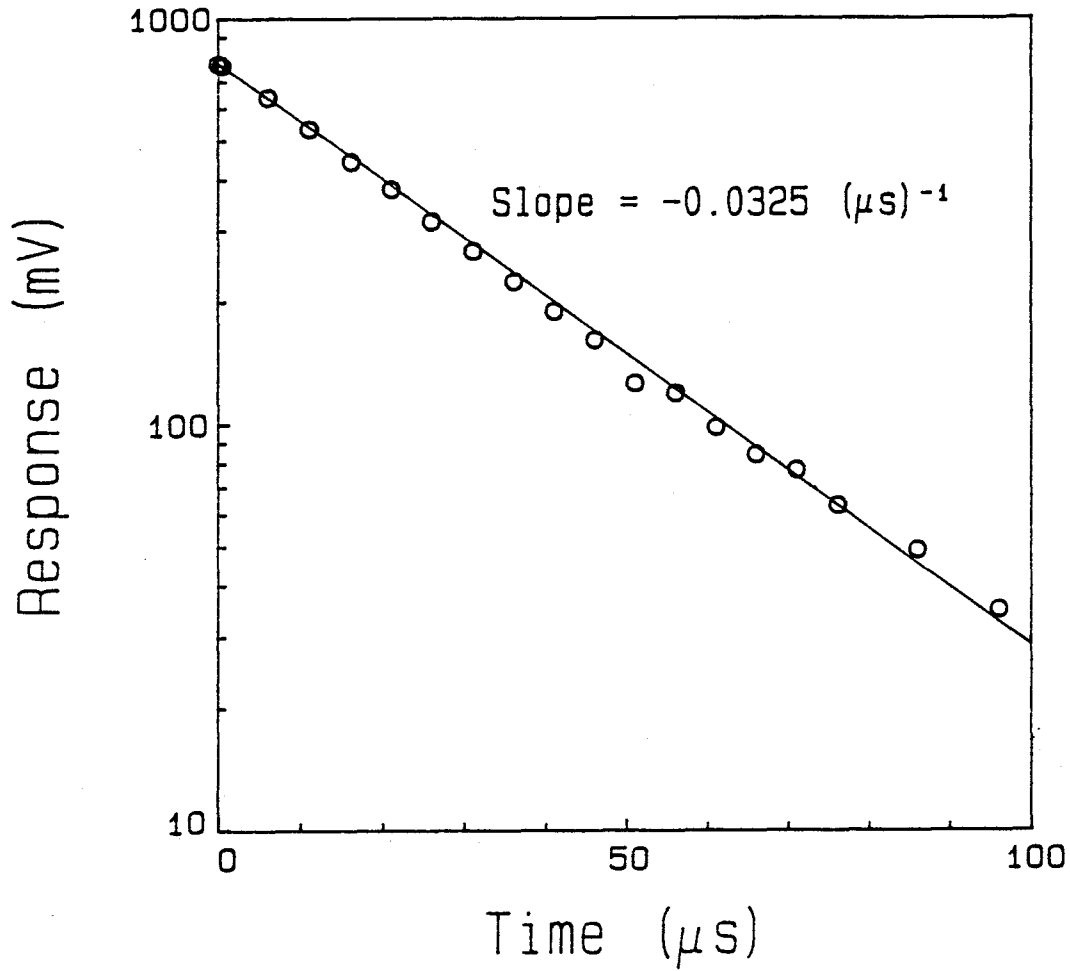


Figure A2 Semilog plot of E0-817S response.

REFERENCES

- Andreoni, A. et al. "Hematoporphyrin Derivative: Experimental Evidence for Aggregated Species". *Chemical Physics Letters*, 88 (1), 33-36, 1982.
- Boulnois, J.-L. "Photophysical Processes in Recent Medical Laser Developments: a Review". *Lasers in Medical Science* 1, 47-66, 1986.
- Bracewell, R.N. The Fourier Transform and its Applications. McGraw-Hill Book Co., New York, 1978.
- Chan, W.S. et al. "Cell uptake, distribution, and response to aluminum chloro sulphonated phthalocyanine, a potential anti-tumour photosensitizer". *British Journal of Cancer*, 53, 255-263, 1986.
- Darwent, J.R. et al. "Excited Singlet and Triplet State Electron-transfer Reactions of Aluminum (III) Sulphonated Phthalocyanine". *Journal of the Chemical Society, Faraday Transactions, II*, 78, 347-357, 1982.
- Dougherty, T.J. "Yearly Review: Photosensitizers: Theory and Detection of Malignant Tumours". *Photochemistry and Photobiology*, 45 (6), 879-889, 1987.
- Firey, P.A. and Rodgers, M.A.J. "Photochemical Properties of Erythrocyte Ghosts Containing Porphyrin". *Photochemistry and Photobiology*, 47 (5), 615-619, 1988.
- Frimer, A.A. Singlet Oxygen Volume I: Physical Chemical Aspects. CRC Press, Inc., Boca Raton, 1985.
- Grossweiner, L.I. "Membrane photosensitization by hematoporphyrin and hematoporphyrin derivative". In Porphyrin Localization and Treatment of Tumors. Doiron, D.R. and Gomer, J. (Eds.). Alan R. Liss, Inc., New York, 1984, pp. 391-404.
- Hurst, J.R. and Schuster, G.B. "Nonradiative Relaxation of Singlet Oxygen in Solution". *Journal of the American*

References (cont.)

- Chemical Society, 105 (18), 5756-5760, 1983.
- Jori, G. and Spikes, J.D. "Photochemistry of Porphyrins". In Topics in Photomedicine. Smith, K.C. (Ed.). Plenum Press, New York, 1984, pp. 183-318.
- Keir, W.F. et al. "Pulsed Radiation Studies of Photodynamic Sensitizers: The Nature of DHE", Photochemistry and Photobiology, 46 (5), 587-589, 1987.
- Kessel, D. "Yearly Review: Hematoporphyrin and HPD: Photophysics, Photochemistry and Phototherapy". Photochemistry and Photobiology, 39 (6), 851-859, 1984.
- Khan, A.N. and Kasha, M. "Direct spectroscopic observation of singlet oxygen emission at 1268 nm excited by sensitizing dyes of biological interest in liquid solution". Proceedings of the National Academy of Science (USA), 76, 6047-6049, 1979.
- Krasnovsky, A.A. "Photosensitized Luminescence of Singlet Oxygen in Solution". Biofizika (USSR), 21, 748-749, 1976.
- Levine, I.N. Quantum Chemistry. Allyn and Bacon, Inc., Toronto, 1983.
- Matheson, I.B.C. et al. "The Quenching of Singlet Oxygen by Amino Acids and Proteins". Photochemistry and Photobiology, 21, 165-171, 1975.
- Moan, J. et al. "The Mechanism of Photodynamic Inactivation of Human Cells in Vitro in the Presence of Haematoporphyrin Derivatives". British Journal of Cancer, 39, 398-407, 1979.
- Morita, H. and Nagakura, S. "Hydrogen-Bonded O-H and O-D Overtone Bands and Potential Energy Curve of Methanol". Journal of Molecular Spectroscopy, 49, 401-413, 1974.
- Parker, J.G. "Optical Monitoring of Singlet Oxygen Generation During Photodynamic Treatment of Tumors". IEEE Circuits and Devices Magazine, January, 10-21,

References (cont.)

1987.

- Parker, J.G. and Stanbro, W.D. "Energy Transfer Processes Accompanying Laser Excitation of Hematoporphyrin in Various Solvents". John Hopkins APL Technical Digest, 2 (3), 196-199, 1981.
- Parker, J.G. and Stanbro, W.D. "Dependence of Photosensitized Singlet Oxygen Production on Porphyrin Structure and Solvent". In Porphyrin Localization and Treatment of Tumors. Doiron, D.R. and Gomer, J. (Eds.). Alan R. Liss, Inc., New York, 1984, pp. 259-284.
- Patterson, M.S. et al. "The Propagation of Optical Radiation in Tissue". In Advances in Laser Biophysics. Colles, M.J. (Ed.). JAI Press, New York, 1988 (in press).
- Poletti, A. et al. "Photophysical and photosensitizing properties of Photofrin II". In Porphyrins in Tumor Phototherapy. Andreoni, A. and Cubeddu, R. (Eds.). Plenum Press, New York, 1984, pp. 37-43.
- Redmond, R.W. et al. "Aggregation Effects on the Photophysical Properties of Porphyrins in Relation to Mechanisms Involved in Photodynamic Therapy". In Methods in Porphyrin Photosensitization II. Kessel, D. (Ed.). Plenum Press, New York, 1985, pp. 293-302.
- Rodgers, M.A.J. "Activated Oxygen". In Primary Photo-processes in Biology and Medicine. Jori, G., Land, E.J. and Truscott, T.G. (Eds.). Plenum Press, New York, 1985, pp. 181-195.
- Rodgers, M.A.J. "On the problems involved in detecting luminescence from singlet oxygen in biological specimens". Journal of Photochemistry and Photobiology, B: Biology, 1 371-373, 1988.
- Rosenthal, I. et al. "The Role of Molecular Oxygen in the Photodynamic Effect of Phthalocyanines". Radiation Research, 107, 136-142, 1986.
- Schmidt, R. et al. "Determination of the Phosphorescence Quantum Yield of Singlet Molecular Oxygen ($^1\Delta_g$)

References (cont.)

- in Benzene". *Chemical Physics Letters*, 138 (1), 18-22, 1987.
- Scurlock, R.D. and Ogilby, P.R. "Effect of Solvent on the Rate Constant for the Radiative Deactivation of Singlet Molecular Oxygen ($^1\Delta O_2$)". *Journal of Physical Chemistry*, 91, 4599-4602, 1987.
- Sinclair, R.S. et al. "The Photophysics and Photochemistry of some Dye Sensitizers". In Photosensitization: Molecular, Cellular and Medical Aspects. NATO ASI Series, H15. Moreno, G. et al. (Eds.). Springer-Verlag, Berlin-Heidelberg, 1988, pp. 53-62.
- Spikes, J.D. and Bommer, J.C. "Zinc tetrasulphophthalocyanine as a photodynamic sensitizer for biomolecules". *International Journal of Radiation Biology*, 50 (1), 41-45, 1986.
- Suit, H.D. "Potential for Survival Rates for the Cancer Patient by Increasing the Efficacy of Treatment of the Primary Lesion". *Cancer*, 50, 1227-1234, 1982.
- Tannock, I. and Hill, R. The Basic Science of Oncology. Pergamon Press, Toronto, 1987.
- Turro, N.J. Modern Molecular Photochemistry. The Benjamin/Cummings Publishing Co., Inc. Menlo Park, 1978.
- van Lier, J.E., et al. "Phthalocyanines for Photodynamic Therapy of Cancer". In Photosensitization: Molecular, Cellular and Medical Aspects. NATO ASI Series, H15. Moreno, G. et al. (Eds.). Springer-Verlag, Berlin-Heidelberg, 1988, pp. 435-444.
- Varani, J. et al. "A Comparison of the Migration Patterns of Normal and Malignant Cells in Two Assay Systems". *American Journal of Pathology*, 90 (1), 159-171, 1978.
- Weishaupt, K.R. "Identification of Singlet Oxygen as the Cytotoxic Agent in Photo-inactivation of a Murine Tumour". *Cancer Research*, 36, 2326-2329, 1976.
- Whitlow, S.H. and Findlay, F.D. "Single and double electronic transitions in molecular oxygen". *Canadian Journal of Chemistry*, 45, 2087-2091, 1966.

References (cont.)

- Wilson, B.C. and Jeeves, W.P. "Photodynamic Therapy of Cancer". In Photomedicine Vol. II. Ben-Hur, E. and Rosenthal, I. (Eds.). CRC Press, Inc., Boca Raton, 1987, pp. 127-177.
- Wilson, B.C. and Patterson, M.S. "The Physics of Photodynamic Therapy". Physics in Medicine and Biology, 31 (4), 327-360, 1986.
- Wilson, B.C. et al. "Chromatographic Analysis and Tissue Distribution of Radiocopperlabelled Haematoporphyrin Derivatives". Lasers in Medical Science, 3 (2), 1988 (in press).